Subseasonal Predictions of Regional Summer Monsoon Rainfall over Tropical Asian Oceans and Land

XIANGWEN LIU

National Climate Center, and Laboratory for Climate Studies, China Meteorological Administration, Beijing, China

SONG YANG

School of Environmental Science and Engineering, and Institute of Earth Climate and Environment System, Sun Yat-sen University, Guangzhou, China

JIANGLONG LI AND WEIHUA JIE

National Climate Center, and Laboratory for Climate Studies, China Meteorological Administration, Beijing, China

LIANG HUANG

Nantong Meteorological Bureau, Nantong, Jiangsu, China

WEIZONG GU

Zaozhuang Meteorological Bureau, Zaozhuang, Shandong, China

(Manuscript received 16 December 2014, in final form 18 August 2015)

ABSTRACT

Subseasonal predictions of the regional summer rainfall over several tropical Asian ocean and land domains are examined using hindcasts by the NCEP CFSv2. Higher actual and potential forecast skill are found over oceans than over land. The forecast for Arabian Sea (AS) rainfall is most skillful, while that for Indo-China (ICP) rainfall is most unskillful. The rainfall–surface temperature (ST) relationship over AS is characterized by strong and fast ST forcing but a weak and slow ST response, while the relationships over the Bay of Bengal, the South China Sea (SCS), and the India subcontinent (IP) show weak and slow ST forcing, but apparently strong and rapid ST response. Land–air interactions are often less noticeable over ICP and southern China (SC) than over IP. The CFSv2 forecasts reasonably reproduce these observed features, but the local rainfall–ST relationships often suffer from different degrees of unrealistic estimation. Also, the observed local rainfall is often related to the circulation over limited regions, which gradually become more extensive in forecasts as lead time increases. The prominent interannual differences in forecast skill of regional rainfall are sometimes associated with apparent disparities in forecasts of local rainfall–ST relationships. Besides, interannual variations of boreal summer intraseasonal oscillation, featured by obvious changes in frequency and amplitude of certain phases, significantly modulate the forecasts of rainfall over certain regions, especially the SCS and SC. It is further discussed that the regional characteristics of rainfall and model's deficiencies in capturing the influences of local and large-scale features are responsible for the regional discrepancies of actual predictability of rainfall.

1. Introduction

The Asian summer monsoon (ASM), one of the most energetic components of the global climate system, influences about half of the world's population by its pronounced multiscale variability and close relationships with many prominent weather and climate phenomena

Denotes Open Access content.

Corresponding author address: Prof. Song Yang, Department of Atmospheric Sciences, Sun Yat-sen University, 135 W. Xingang Rd., Haizhu District, Guangzhou, Guangdong 510275, China.
E-mail: yangsong3@mail.sysu.edu.cn

DOI: 10.1175/JCLI-D-14-00853.1

both inside and outside the monsoon region. Thus, understanding the origin of monsoon variability and further providing accurate prediction of monsoon climate especially monsoon rainfall are of critical importance for the development of economy and society.

Over the past few decades, dynamical forecast has achieved a great progress and become an important approach in monsoon research and prediction operation. With the upgrade of dynamical models (Arribas et al. 2011; Molteni et al. 2011; Saha et al. 2014), enhancement of model resolutions (Pope and Stratton 2002; Wen et al. 2012), improvement of initial conditions (Fu et al. 2009, 2011), inclusion of air–sea coupling (Krishna Kumar et al. 2005; Wang et al. 2005), application of ensemble methods (Wang et al. 2009; Weisheimer et al. 2009; Kirtman et al. 2014), and utilization of the downscaling method (Kang et al. 2009; Sun and Chen 2012), the skill in predicting monsoon and its influencing factors has been improved. However, apparent deficiencies in reproducing the observed monsoon climatology, variability, and relationships with other climate systems still exist in the state-of-the-art climate models (Wang et al. 2008; Lee et al. 2010; Kim et al. 2012; Liu et al. 2013; Zhao and Yang 2014). Especially, dynamical predictions are often less skillful in capturing regional monsoon characteristics compared to large-scale features and in describing monsoon rainfall compared to monsoon circulation (Yang et al. 2008; Drbohlav and Krishnamurthy 2010; Liu et al. 2014a, 2015; Jiang et al. 2013a).

Subseasonal forecast of ASM, with a focus on the extended range time scale between weather phenomena and seasonal means, is noticeably controlled by both initial conditions and boundary forcing, and is thus an especially challenging task. The subseasonal predictability of tropical monsoon rests largely on the existence of low-frequency tropical intraseasonal oscillations (Waliser et al. 2003; Pegion and Sardeshmukh 2011). In spite of many shortcomings, present climate models have shown reasonable prediction skill in reproducing the major features of intraseasonal oscillations including their structure, intensity, spectrum, propagation, and relationships with seasonal-to-interannual climate variability (e.g., Kim et al. 2008; Xavier et al. 2008; Seo et al. 2009; Joseph et al. 2010; Fu et al. 2011; Liu et al. 2014b). Some global models exhibit useful skill on time scales beyond 2–3 weeks, especially when measured by indices of multivariate spatial modes (Fu et al. 2013a; Neena et al. 2014). It is also noted that intraseasonal rainfall variability is often more difficult to predict compared to circulation variability (Reichler and Roads 2005; Fu et al. 2011, 2013b). Many studies have focused on the forecast skill of intraseasonal oscillations over extensive tropical domains instead of regional features. Recently Abhilash et al. (2014) and Liu et al. (2014a) have examined the subseasonal prediction skill for the Indian monsoon and the major global monsoon components, respectively, and found that the actual forecast skill is closely related to the behaviors of large-scale features that are linked to regional monsoons. Nevertheless, there are still few particular explorations on subseasonal forecasts of rainfall over different regions that are important aspects to address in this study.

Air–sea interaction over the tropical Indo-western Pacific contributes significantly to subseasonal monsoon variability (Hendon and Glick 1997; Woolnough et al. 2000). Ocean–atmosphere coupling apparently affects the characteristics of subseasonal anomalies, especially their amplitude and propagation (Waliser et al. 1999; Fu et al. 2003; Pegion and Kirtman 2008). As a critical process, the mutual feedback between subseasonal sea surface temperature (SST) and rainfall over the tropical Indo–western Pacific has been explored using both observed and simulated data (Hendon and Glick 1997; Woolnough et al. 2000; Arakawa and Kitoh 2004; Pegion and Kirtman 2008). Its regional features and differences have also been investigated (Roxy and Tanimoto 2007, 2012; Wu et al. 2008; Wu 2010). Roxy et al. (2013) examined the discrepancies in ocean–atmosphere and atmosphere–ocean effects over three different ocean areas in the tropical ASM region and explained local SST–rainfall relationships. However, most previous studies often focus on the overall characteristics rather than the interannual difference in subseasonal predictability and the possible effect of air–sea interaction on actual predictions of subseasonal monsoon rainfall variability. Also, the regional differences in rainfall–surface temperature (ST) interaction over land are less discussed compared to those over oceans.

Given the above aspects to address, we conduct this study with a particular concern on the subseasonal forecast of ASM regional rainfall using hindcasts from a state-of-the-art climate forecast model. The rainfall over the Arabian Sea (AS), the India subcontinent (IP), the Bay of Bengal (BOB), Indo-China (ICP), the South China Sea (SCS), and southern China (SC) are focused. The following questions are particularly addressed: At what lead time can the subseasonal regional rainfall variability be predicted? To what extent can local sea/land–air interactions and large-scale circulation pattern be skillfully reproduced and how are they responsible for the performance of rainfall forecasts? What are the differences among the various regions, and between land and ocean domains? What are the possible causes of these differences?

The rest of this paper is organized as follows. An overview of model output and observational data is provided in section 2. Subseasonal predictions of the general

characteristics and regional features are given in sections 3 and 4. Prediction of local ST–rainfall relationship and its influence on rainfall forecast are examined in section 5. Modulation of the boreal summer intraseasonal oscillation (BSISO) on regional rainfall forecast is explored in section 6. A summary and a discussion of the results obtained are provided in section 7.

2. Data and analysis methods

The hindcast data from the National Centers for Environmental Prediction (NCEP) Climate Forecast System, version 2 (CFSv2), is used in this study. The CFSv2 is a coupled atmosphere–ocean–land–sea ice dynamical seasonal prediction system (Saha et al. 2014). It comprises the NCEP atmospheric Global Forecast System with a spectral triangular truncation at wavenumber 126 (T126) horizontal resolution and 64 sigma layers in the vertical, the four-layer Noah land surface model, and the Geophysical Fluid Dynamics Laboratory Modular Ocean Model, version 4, at 0.25°–0.5° grid spacing coupled with a two-layer sea ice model. The CFSv2 has provided rolling retrospective forecasts with 45-day integrations initiated from every 0000, 0600, 1200, and 1800 UTC cycle from 1999 to 2010. The daily-mean output for rainfall, winds, ST, and outgoing longwave radiation (OLR) is analyzed in this study.

The observational data used for model verification include the daily winds and ST from the NCEP Climate Forecast System Reanalysis (CFSR; Saha et al. 2010; http://cfs.ncep.noaa.gov/cfsr/) with a 1° × 1° horizontal resolution, precipitation from the Global Precipitation Climatology Project (GPCP; Huffman et al. 2001; http://precip.gsfc.nasa.gov/) at 1° × 1° resolution, and OLR (Liebmann and Smith 1996; http://www.esrl.noaa.gov/psd/data/gridded/data.interp_OLR.html) from the National Oceanic and Atmospheric Administration (NOAA) at 2.5° × 2.5° resolution. Based upon interpolations of data from high to low resolution with area-weighting interpolation method, the computations in sections 3–5 are conducted on a 1° × 1° resolution that is consistent with CFSR, while the calculations for BSISO modes in section 6 are carried on a 2.5° × 2.5° resolution for unification with NOAA OLR.

In our study, results of subseasonal prediction are mostly examined by pentad means of various variables in boreal summer (June–September), except that the BSISO features shown in section 6 are based on daily means. For a specific target pentad, lead 0 denotes the forecasts initialized on the first day of the pentad, lead 1 refers to the forecasts initialized on the last day of the previous pentad, lead 2 for the model runs initialized 2 days ahead of the first day of the target pentad, and so forth. To reasonably show ensemble prediction skill, the predictions for a certain pentad are divided into 22 groups according to the length of lead time (i.e., 0–1, 2–3, and every 2 days to 42–43 days). Thus, most of the pentad predictions are ensemble means of eight members within 2-day leads. For each pentad in a certain year, and for all the lead days, the pentad-mean anomalies are computed by subtracting the corresponding pentad climatology from 1999 to 2010 and further deducting the seasonal mean anomaly of that year, thus retaining the climate variability signals between synoptic and seasonal time scales.

3. Prediction of major rainfall features over ASM regions

Liu et al. (2013, 2014a) have reported bias formation of the ASM in the CFSv2. Significant systematic biases of monsoon rainfall exist in the model, including wet biases over the AS, the equatorial Indian Ocean, and the tropical western North Pacific and dry biases over the IP, ICP, northern BOB, and the SCS. In association, westerly wind bias occurs over the equatorial Indian Ocean and easterly wind bias appears over southern Asia. A cyclonic wind bias dominates over the northwestern Pacific and a northerly wind bias prevails over the SCS. For ST, warmer biases are found over the AS, BOB, SCS, and the tropical western North Pacific, and cooler biases appear over the ICP and SC, with opposite-sign biases to the north and south of IP. Various biases are closely associated with internal and external factors of the atmosphere, and they often show time dependence.

Underestimation of rainfall over the northern BOB and SCS and overestimation of rainfall over the western North Pacific have also been found in the NCEP CFS, version 1 (e.g., Yang et al. 2008; Drbohlav and Krishnamurthy 2010), DEMETER, and ENSEMBLES multimodel seasonal forecasts (e.g., Preethi et al. 2010; Rajeevan et al. 2012), and the prediction models of the Asian–Pacific Economic Cooperation (APEC) Climate Center/Climate Prediction and its Application to Society (APCC/CliPAS) projects (Lee et al. 2010). Different from the opposite biases over the eastern and western equatorial Indian Ocean in the CFS, version 1, and other multimodel ensemble forecasts (Drbohlav and Krishnamurthy 2010; Rajeevan et al. 2012), the CFSv2 exhibits an extensively wet bias over the entire equatorial Indian Ocean. In addition, as in most climate models, excessive rainfall is predicted over the west coast of ICP and the southern flank of the Tibetan Plateau, attributed possibly to the model's inability in describing terrain-related rainfall. These biases suggest some common deficiencies of monsoon rainfall forecast by current climate models.

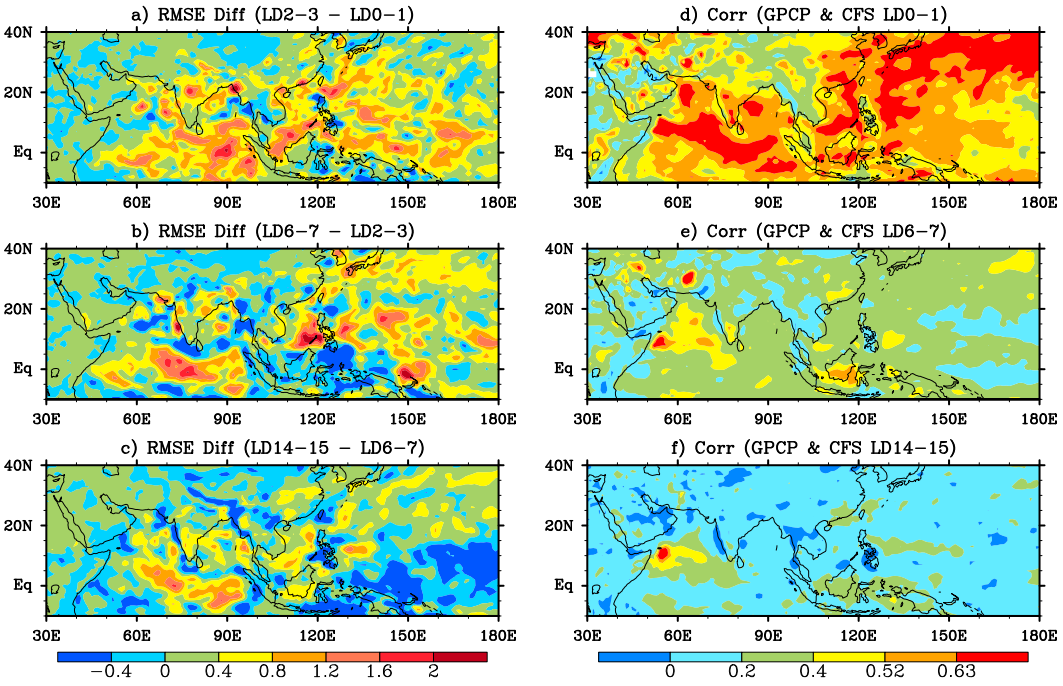

FIG. 1. (left) Differences in root-mean-square error of rainfall (mm day^{-1}) between leads of (a) 2–3 and 0–1 days, (b) 6–7 and 2–3 days, and (c) 14–15 and 6–7 days. (right) Temporal correlations between observation and predictions of leads of (d) 0–1, (e) 6–7, and (f) 14–15 days. Shown are the 12-year means from 1999 to 2010. The shading levels of 0.4, 0.52, and 0.63 at (right) represent the statistically significant values of correlation above the 95%, 99%, and 99.9% confidence levels, respectively.

The standard deviation of subseasonal rainfall variation is also explored. Different from the significant seasonal-to-interannual variability over the ASM region and equatorial regions (e.g., Drbohlav and Krishnamurthy 2010; Kim et al. 2012), maximum subseasonal variations of rainfall are observed over eastern AS, northern BOB, SCS, and the Philippine Sea. This feature appears because of the prevalence of intraseasonal oscillation, a major part of subseasonal variability, over the tropical ASM region in summer (e.g., Kim et al. 2008; Joseph et al. 2010). The CFSv2 predictions capture the general spatial distribution of the major centers, but with apparently overestimated magnitude at the minimum lead time. On the other hand, the values over the mainland of ASM region are often underestimated. As lead time increases, the standard deviations of regional rainfall exhibit an abruptly decreasing tendency, due partially to the saturation and little change of model error at the high leads, as well as the gradually increasing contribution from the slowly varying components of the large-scale climate system (figure not shown).

Based on the root-mean-square error (RMSE) and temporal correlation coefficient (TCC) between observations and predictions, we present the spatial distributions of multiyear-averaged skill in subseasonal rainfall variation in Fig. 1. Remarkable differences in RMSE between forecasts of 2-day lead and 0-day lead appear over most of the tropical central-eastern Indian Ocean and the northwestern Pacific, denoting a quick formation of error over the tropical ASM region at short leads. When lead time advances, the range of marked increase in RMSE shrinks gradually and is confined to the equatorial central-eastern Indian Ocean at about a 2-week lead. Nevertheless, over regions such as the southwest and northeast coast of AS and the western equatorial Pacific, RMSE decreases from a 1-week lead to a 2-week lead (Figs. 1a–c). Because of the much quicker saturation of error for rainfall than for circulation, error growth of rainfall is often very small after the 2-week lead. Also, in spite of a quick decrease in TCC with lead time, more significant skill is found over oceans than over land. Especially, the forecast of rainfall over the AS is more skillful than that over other oceans (Figs. 1d–f). Similarly, prediction of 850-hPa zonal wind shows especially high skill over the AS and south of the ICP and SCS, and forecast of ST is often more skillful over the AS than over the BOB, the equatorial eastern Indian Ocean, and the SCS (figures not shown).

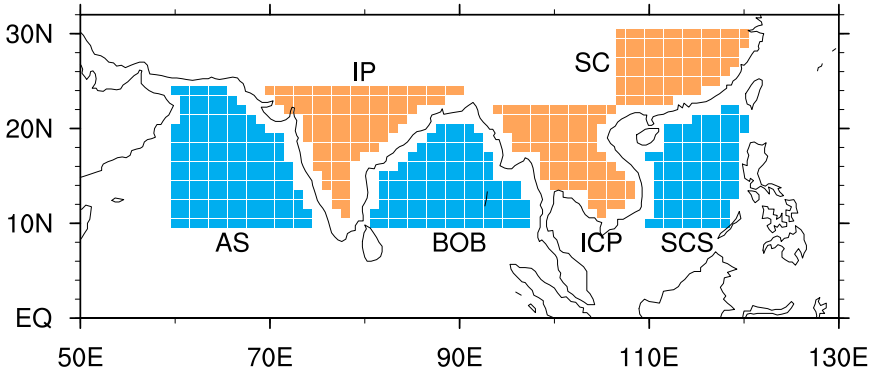

FIG. 2. Ranges of ocean domains (blue; Arabian Sea, Bay of Bengal, and South China Sea) and land domains (brown; India subcontinent, Indo-China, and southern China) defined in this study.

4. Prediction of regional monsoon rainfall

a. Selection of ocean and land domains

We determine the domains of analysis based on both their geographical locations and the distributions of rainfall climatology and variability. The details of domain-selecting process are described as follows. First, with an area-weighting interpolation method, the 2′ gridded global relief data, ETOPO2v2, are interpolated to the horizontal grids used in our analysis to obtain a real ocean–land mask. Then, the general ranges of several tropical Asian ocean and land domains are listed according to their locations and rainfall features. At last, given the difficulty in estimating the influence of topography on rainfall by climate models and models' inability of describing the effect of local ocean–land difference resulting from limited resolution and problem of ocean–land mask, we further remove some grid points near the ocean–land boundaries and ensure that all the others in a certain ocean/land domain are enclosed by grids with the same nature. The final ranges of various ocean and land domains are drawn in Fig. 2.

The subseasonal variations of area-averaged rainfall climatologies for the various domains are given in Fig. 3. Most predictions of rainfall over AS and IP are featured by obvious wet and dry biases during the entire summer, respectively. Compared to the overall small differences among various leads of rainfall predictions over AS and most lands, remarkable spreads of ensemble members exist in the predictions over BOB and SCS, suggesting large potential uncertainties for rainfall forecasts over the latter two regions. For the temporal evolution of climatological rainfall, high and slowly decreasing correlations between observations and multilead predictions are found over AS, IP, and SC, in contrast to the low and quickly dropping correlations over BOB, SCS, and ICP. This feature appears partially because the climatological rainfall over the former three regions has a significant seasonal trend in summer, which is more easily captured by the model. Meanwhile, the large subseasonal variance and notable forecast spread over SCS and BOB also cause difficulty in predicting the seasonal cycle of rainfall over these two areas.

b. Skill in spatial and temporal variability of regional rainfall

For the rainfall anomalies over various regions, pattern correlation coefficient (PCC) between observation and prediction is computed pentad by pentad, and year by year. The multiyear-averaged PCC in each pentad and the summer-averaged PCC in each year are given in Fig. 4. In respect to the climatological average, overall higher skill is found for forecasts of rainfall over oceans than over land (Fig. 4a). Especially, the forecasts of rainfall over ICP are mostly unskillful during the entire summer. It should also be noted that the rainfall over oceans, especially the AS and the SCS, exhibits a minimum of PCC from mid-July to early August, which to some extent agrees with the findings by Fu et al. (2011) and Abhilash et al. (2014). Forecasts of rainfall over oceans exhibit more remarkable interannual differences, featured by a drop of PCCs below the 95% confidence level after a few days of forecasts in some time but at about three-week or longer lead in other time (Fig. 4b). The maximum lead time for forecasts with useful skill is 27, 21, and 19 days, and the minimum lead time is 3, 5, and 3 days for predictions of rainfall over AS, BOB, and SCS, respectively (Table 1). In contrast, relatively small interannual differences of PCC are found for forecasts over most land domains, along with rapid descents of PCC below the confidence level in most cases (Fig. 4b). The longest lead time for skillful forecasts of rainfall over IP, ICP, and SC is

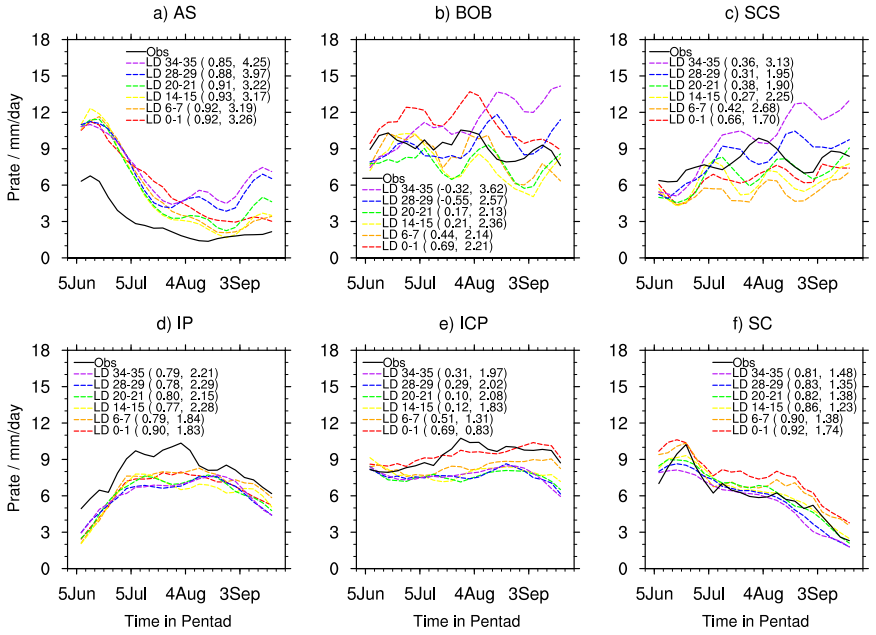

FIG. 3. Pentad climatologies of rainfall (mm day^{-1}) averaged over the (a) Arabian Sea, (b) Bay of Bengal, (c) South China Sea, (d) India subcontinent, (e) Indo-China, and (f) southern China for observation and forecasts of various leads. All lines are smoothed by three-point running average, and the decimal values shown in parentheses represent the temporal correlations and root-mean-square errors between observation and predictions.

9, 5, and 11 days, and the shortest is 0 day for IP and ICP rainfall and 1 day for SC rainfall (Table 1). Meanwhile, Fig. 4b and Table 1 also present the potential forecast skill over various regions that are defined as the correlations between two different forecasts at certain lead time assuming that the model is perfect. On average, the potential forecast skill is significant at the lead time of about 40 days for rainfall over all oceans, but become unskillful beyond the lead time of about 3 weeks for the rainfall over IP and ICP and 2 weeks for the rainfall over SC. The actual forecasts are obviously worse than the potential forecasts of rainfall, especially over ICP where the largest potential skill and smallest actual skill among three land domains are found.

We further examine the TCCs of subseasonal rainfall variations over the various domains (Fig. 5a). Similar to PCCs, the TCCs over oceans decrease more slowly with lead time and exhibit larger interannual differences over oceans than over land. TCCs and PCCs of rainfall overall show different interannual features. However, for some extreme cases such as the skillful forecasts of the AS rainfall in 2000 and 2006 and the SCS rainfall in 2007, as well as the unskillful forecasts of the AS rainfall in 2007, the BOB rainfall in 2009, and the SCS rainfall in 2010, TCCs and PCCs can attain skill peaks or lows simultaneously. This feature suggests the possible existence of certain predictability factors that commonly affect the temporal and spatial variability of rainfall in some particular years. In addition, the average lead time for TCC to become insignificant is the longest for the AS rainfall (beyond 11 days) and the shortest for the ICP rainfall (beyond 1 day), respectively. Especially, the rainfall over AS can be predicted skillfully at the lead time of 27 days in 2003, but the rainfall over ICP cannot be captured even at a 0-day lead time in 1999, 2005, and 2007 (Table 1). These results further demonstrate the especially reasonable skill in forecasting the rainfall over AS and the tremendous difficulty in forecasting the rainfall over ICP. Much better than the actual forecasts, potential forecasts show useful skill at lead time above 40 days for rainfall over oceans, but are skillful only at lead time shorter than 3 weeks for rainfall over land, with a minimum of 17 lead days over SC (Fig. 5a, Table 1).

To understand the relationship between tropical rainfall and the underlying ST, we also analyze the TCCs of subseasonal variations of the average ST over different regions (Fig. 5b). Apparent interannual differences in forecasts, especially at long leads, are found over most domains except SC. On average, the lead days for forecast skill to fall below the confidence level of statistical significance are around 2 weeks over most regions except AS where the forecasts with leads of above 3 weeks are still skillful. The average potential

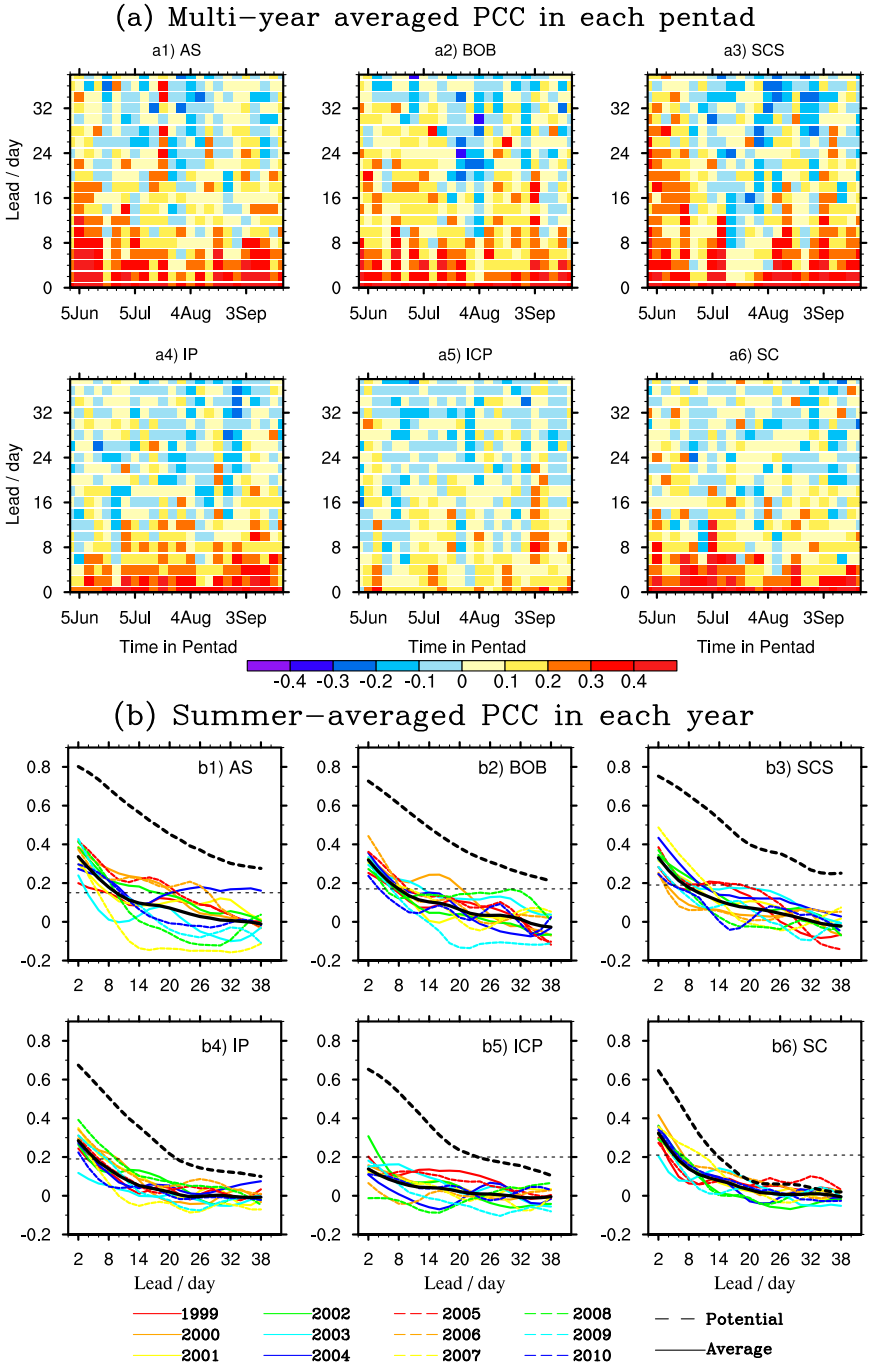

FIG. 4. (a) Multiyear-averaged pattern correlations of rainfall anomalies over various regions between observation and forecasts as a function of lead time (*y* coordinate) and seasonal stage (*x* coordinate). (b) Summer-averaged pattern correlations as a function of lead time (*x* coordinate) for each year. Results shown in (b) are three-point running averages along the forecast lead time, and the black dashed straight lines denote the values of statistical significance at the 95% confidence level. The black solid and dashed curved lines represent the multiyear averages of actual forecast skill and potential skill, respectively.

TABLE 1. The longest lead time (day) for forecasts of regional pentad rainfall with skillful PCCs and TCCs in each year. The right two columns show the longest leads for multiyear averages of actual skill and potential skill, respectively. Eight ensemble members within 2-day leads are used to compute the potential skill based on perfect model assumption.

		1999	2000	2001	2002	2003	2004	2005	2006	2007	2008	2009	2010	Actual	Potential
PCC	AS	7	21	7	17	3	11	21	27	5	9	9	11	9	40
	BOB	7	21	9	7	13	9	9	9	11	5	7	5	7	40
	SCS	5	3	9	11	9	11	19	3	11	7	5	5	7	40
	IP	3	9	7	3	0	5	7	7	5	9	7	3	5	21
	ICP	3	1	0	5	0	1	1	0	0	0	0	0	0	23
	SC	3	7	5	7	1	5	3	5	11	7	5	5	5	13
TCC	AS	5	19	11	9	27	13	7	21	7	9	23	13	11	40
	BOB	15	9	7	9	7	9	11	5	17	5	5	5	7	40
	SCS	9	19	13	3	5	3	5	3	15	5	5	3	5	40
	IP	7	7	1	5	1	5	5	5	5	3	9	9	5	21
	ICP	0	5	1	3	3	7	0	9	0	1	1	7	1	19
	SC	3	5	5	11	9	7	7	9	7	7	9	11	7	17

skill is often significant at a 40-day lead time for the forecasts of ST over most regions except SC, where the longest lead time with useful skill is shorter than 3 weeks. This feature suggests a relatively small difference between potential and actual forecasts of the ST over SC. However, the skillful forecasts of regional ST do not guarantee successful predictions of regional rainfall. For instance, over AS, interannual variations of TCC skill in ST and rainfall do not show significant positive correlations at most leads, and particularly the extremely skillful forecasts of ST at all leads in 2004 and 2005 do not lead to outstanding skill in rainfall predictions [Fig. 5b(1)]. Similar features are also found for forecasts of rainfall over other regions, suggesting that there is probably no significant linear relationship between forecast skill in temporal variations of rainfall and ST over most ASM regions.

To further explore the possible connections among the forecast skill of rainfall and ST, we examine the scatter distributions of TCCs and PCCs of rainfall and ST over various regions. It can be seen from Fig. 6 that overall the various skills are featured by scattered distributions and do not show strong linear relationships. Compared to the relationships between ST PCC and rainfall PCC (Figs. 6c and 6d), and between ST TCC and rainfall TCC (Figs. 6e and 6f), the connection between rainfall TCC and rainfall PCC (Figs. 6a and 6b) often shows even weaker linear relationships, with larger spreads over land than over oceans. Maximum spreads appear over ICP while minimum spreads are over AS. This feature further confirms that overall the temporal variability and spatial variability of regional rainfall cannot be predicted well consistently, in spite of a few exceptions as previously mentioned. In contrast, it is more likely that skillful forecasts of regional ST are related to successful forecasts of rainfall and thus relatively small spreads of linear relationships between ST skill and rainfall skill are often found (Figs. 6c–f), except for the forecasts of ST and rainfall over BOB (Fig. 6c). Given the overall insignificant correlation between ST TCC and rainfall TCC shown above, the relatively strong relationship between the forecasts of ST and rainfall is more exemplified in capturing their PCCs. Especially, the interannual correlations between the PCCs (average during 0–10 lead days) of ST and rainfall over SCS and IP are 0.63 and 0.73, respectively, both above the 95% confidence level.

5. Effects of local ST–rainfall relationship

To understand the possible causes of the success or the failure of regional rainfall forecasts, subseasonal sea–air interaction and land–air interaction and their influences on regional rainfall are examined, with a focus on the observed and predicted relationships between rainfall and ST over various regions as well as their regional differences. The features of related large-scale circulation are also discussed.

The simultaneous relationships of area-averaged rainfall with ST and 850-hPa winds over the ASM region are given in Fig. 7. In observation, heavy rainfall over AS corresponds to a cyclonic wind anomaly from Somali to northern AS, associated with warm (cool) ST over the north (south) of maximum wind anomaly. The CFSv2 reasonably reproduces the observed features at lead time shorter than two weeks, but apparently overestimates the positive correlations between rainfall and ST over an extensive region from AS to the Philippine Sea at longer leads, along with an intensification of zonal wind response over the South Asian monsoon region (Fig. 7a). Also observed is that heavy rainfall over BOB and SCS are coupled with cyclonic wind anomalies over

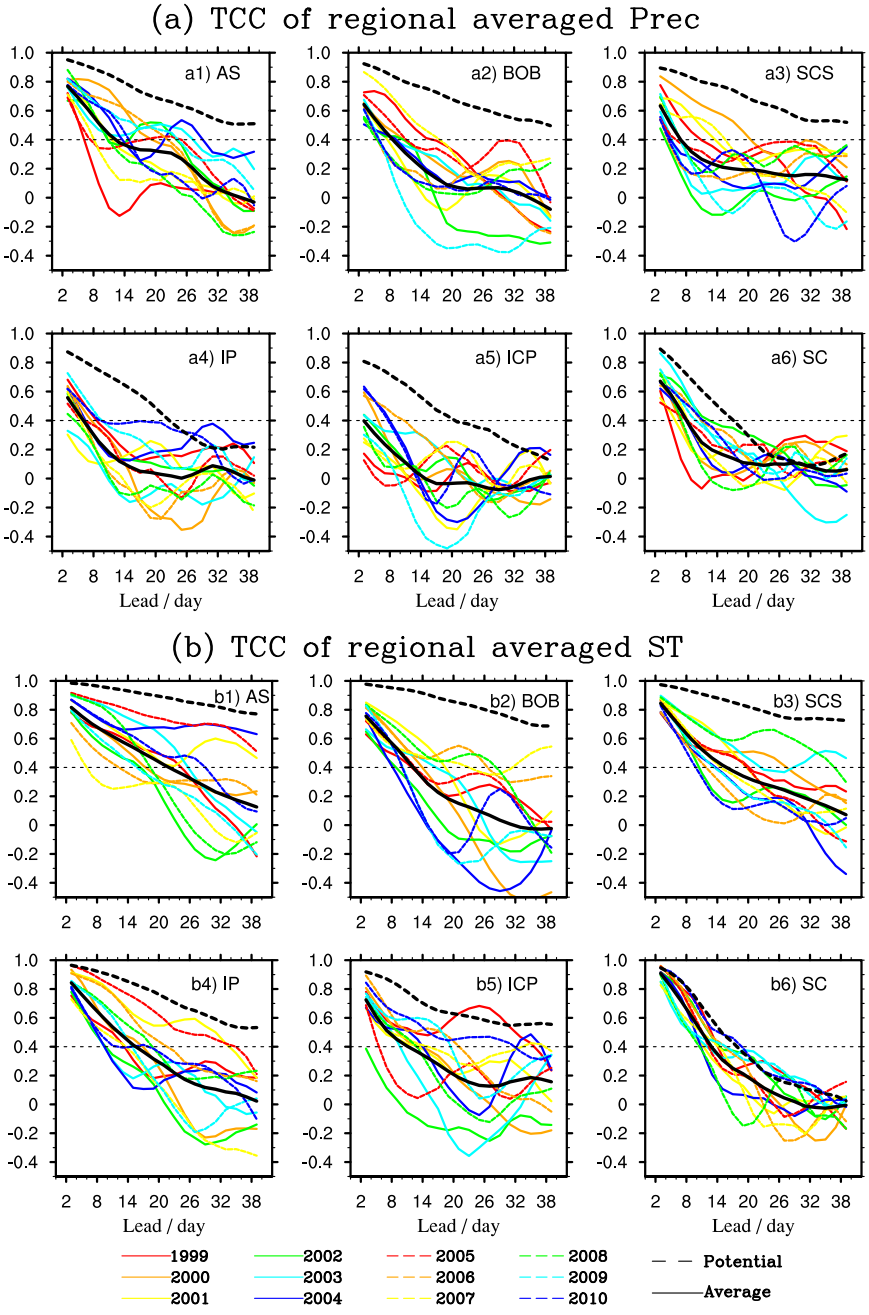

FIG. 5. As in Fig. 4b, but for subseasonal temporal correlations of regionally averaged (a) rainfall and (b) surface temperature between observations and forecasts during the summer. The black dashed straight lines denote the values of statistical significance at the 95% confidence level.

regions from eastern AS to BOB and from BOB to SCS, respectively. These relationships are well captured by the model predictions of short leads, but exaggerated as lead time increases. As a result, a response of zonal wind over a broad region from AS to the Philippine Sea and extensive negative correlations with the ST over tropical Asia, together with regional positive correlations with the ST over south of the Tibetan Plateau, are predicted in the long-lead forecasts for rainfall over both BOB and SCS (Figs. 7b and 7c). The above results indicate gradually strengthening relationships between regional rainfall and large-scale circulation and ST patterns with increasing lead time, especially for rainfall over BOB and SCS, associated with the enhancing connection of

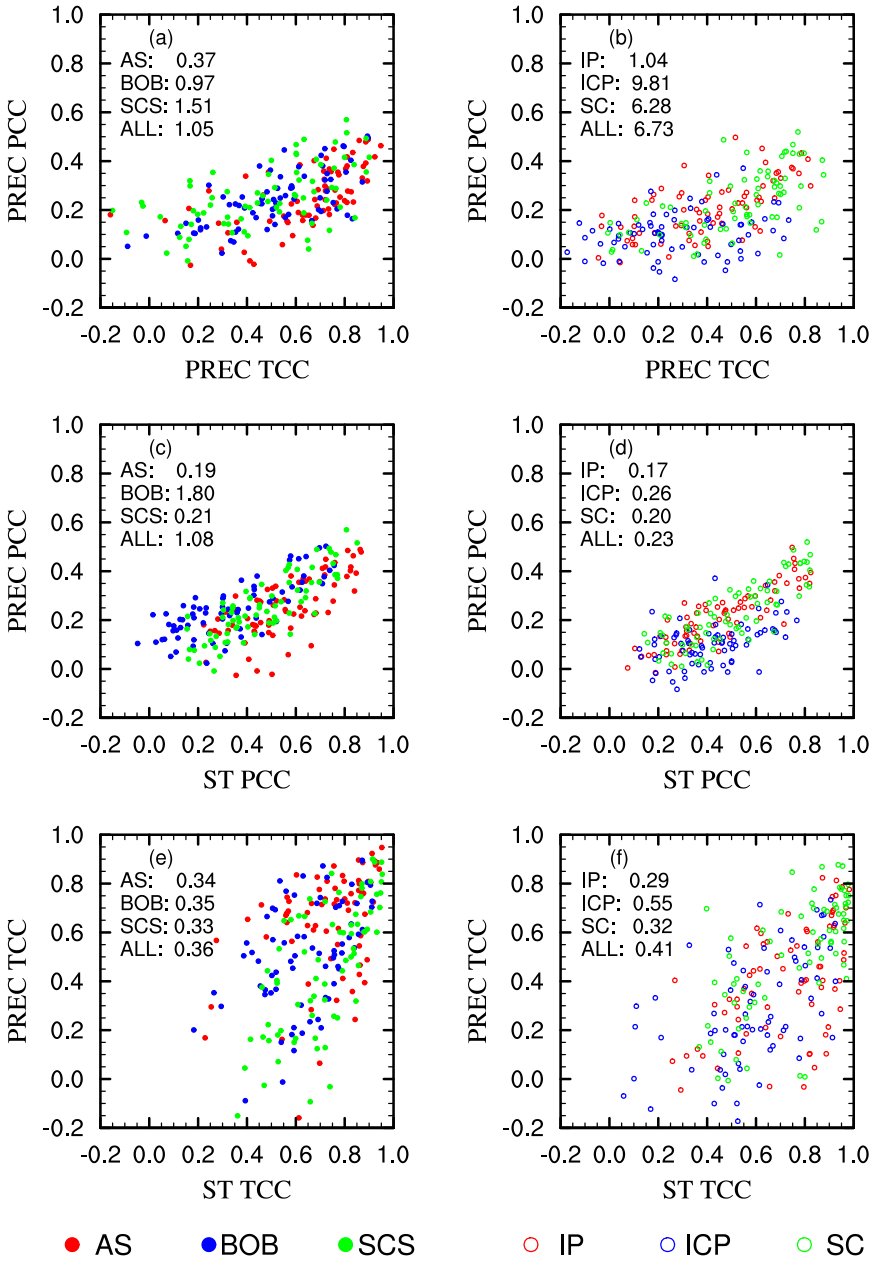

FIG. 6. Scatter distribution of forecast skill for the relationships between (a),(b) TCC and PCC of rainfall; (c),(d) surface temperature PCC and rainfall PCC; and (e),(f) surface temperature TCC and rainfall TCC over (left) oceans and (right) land. Shown are results for forecasts of 0–10 lead days in each year. The decimal values given in each panel are spreads of the ratio of y coordinate to x coordinate for results over Arabian Sea, Bay of Bengal, South China Sea, and all oceans at (left), and for India subcontinent, Indo-China, southern China, and all land at (right), respectively.

rainfall between the two regions as lead time increases. Indeed, the climatological TCC of rainfall between BOB and SCS is only 0.23 in observations, but above 0.5 in forecasts of leads longer than 10 days, with a maximum of 0.7 at the lead of 36 days. This feature denotes that, in long-lead forecasts, the detailed regional difference between BOB and SCS becomes hardly distinguishable.

The rainfall over land always shows insignificant or localized links with 850-hPa winds in both observations and most predictions, and the rainfall over IP and ICP exhibits unrealistically strong connections with regional

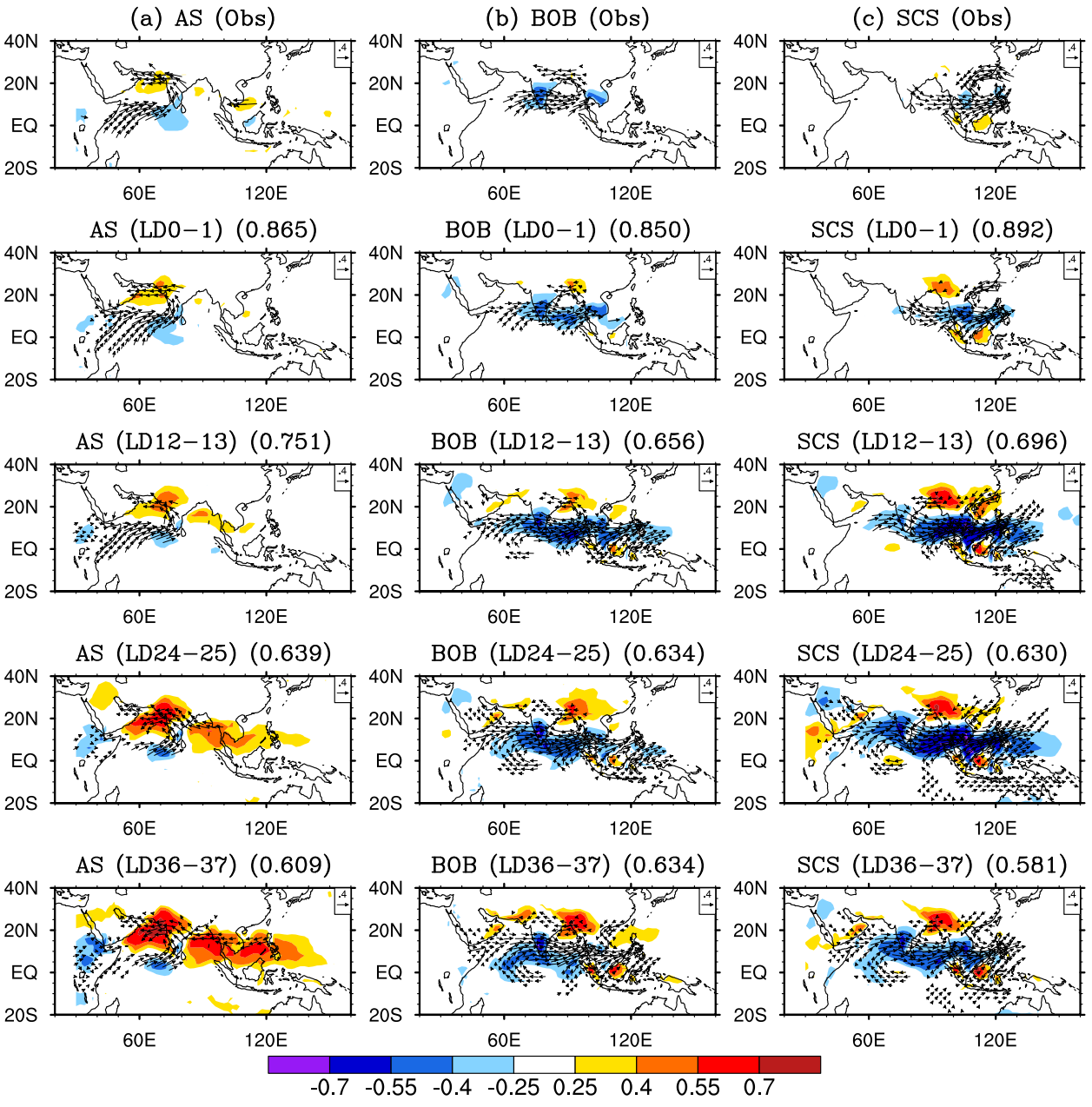

FIG. 7. Patterns of subseasonal temporal correlations (shading) between surface temperature and regional average rainfall, and patterns of regressions (vectors) of 850-hPa winds on regional average rainfall, over the (a) Arabian Sea, (b) Bay of Bengal, and (c) South China Sea. (top)–(bottom) The 12-yr-average features for observations and predictions of different leads. The shading levels of 0.4 and the vectors represent the statistically significant values above the 95% confidence levels. Decimal values given in parentheses on the right in the subtitles are spatial pattern correlations between predicted and observed features.

ST in CFSv2. As lead time increases, the rainfall over IP and ICP, especially the latter, show gradual reinforcing relationships with rainfall over neighboring regions (figures not shown). These features may partially lead to the quick decrease of forecast skill for rainfall over land.

It is also seen from Fig. 7 that on average rainfall and ST show a positive correlation over AS. The feature denotes the leading role of increased ST, induced by downward shortwave radiation flux and suppressed surface latent heat flux, in enhancing convective rainfall by destabilizing the lower atmosphere (Fu et al. 2008; Roxy and Tanimoto 2007, 2012; Wu 2010; Roxy et al. 2013) and modifying the low-level convergence (Waliser et al. 1999; Seo et al. 2007; Fu et al. 2008; Wu 2010). This is different from the features over BOB and SCS where negative correlations are observed, indicating the active

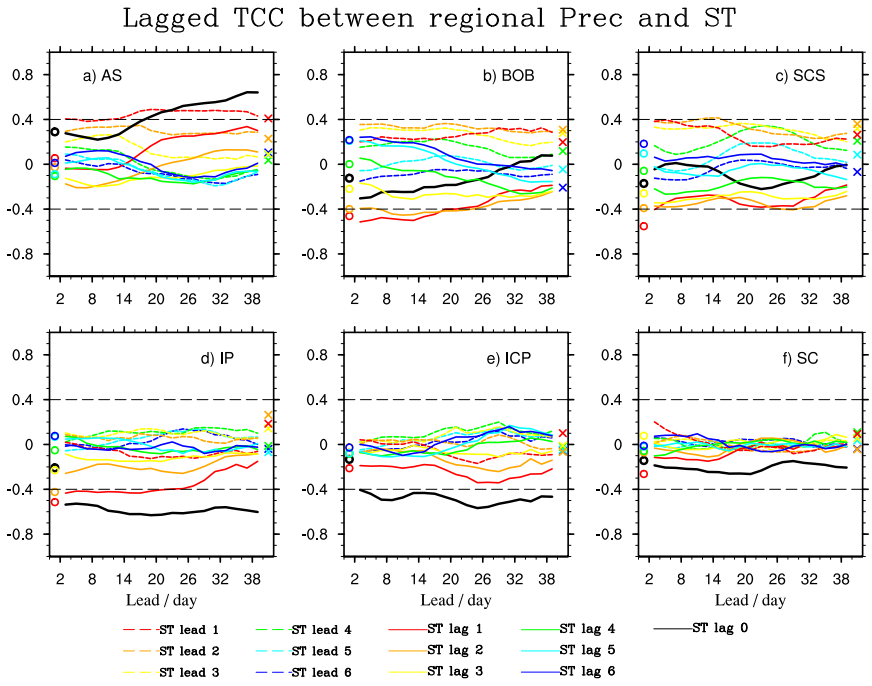

FIG. 8. Multiyear-averaged temporal correlations of regional average rainfall with surface temperature of a 6-pentad lead to a 6-pentad lag over various regions. Curves show the variations of forecasts with lead time, and open circles and crosses (only refer to the *y* coordinate) denote the observations corresponding to the same-color solid lines and dashed lines, respectively. Shown are the three-point running averages along the forecast lead days, and thin black dashed horizontal lines denote the values of statistical significance of correlation at the 95% confidence level.

part of enhanced rainfall in decreasing ST via the decline of shortwave radiation and an increase in surface latent heat (Woolnough et al. 2000; Pegion and Kirtman 2008; Wu 2010; Roxy and Tanimoto 2012; Roxy et al. 2013). Nevertheless, over the three ocean regions, the synchronous TCCs between rainfall and ST are all weak in observations, and they often remain insignificant in most forecasts for BOB and SCS but become significant in the long-lead forecasts for AS.

Figure 8 further shows the lagged TCCs between rainfall and ST for various regions. In observations, maximum and minimum TCCs appear when ST anomalies lead or lag rainfall anomalies by 1–2 pentads. Over AS (Fig. 8a), rainfall is significantly and positively correlated with the ST of 1-pentad lead, while the rainfall–ST correlation quickly decreases and changes into extremely small negative values when ST lags rainfall by 2 pentads or more, implying that the sea–air interaction over AS is more predominated by an ocean–atmosphere effect. By comparison, the rainfall over BOB, SCS, and IP (Figs. 8b–d) is correlated positively with the lead ST by 1–3 pentads, and negatively with the lag ST by 1–3 pentads with a significant minimum at the 1-pentad lag. The result demonstrates the existence of interaction process in which ST affects rainfall and in turn the latter feedbacks onto the former. Overall the leads and lags with maximum and minimum correlations shown in this study agree with the result by Roxy et al. (2013), who showed that the ST leads with the strongest forcing were 5 days for AS and 12 days for BOB and SCS, and the ST lags with the strongest response were 15 days over AS and 7 days over BOB and SCS. Wu et al. (2008) also revealed similar leads of ST forcing over these three ocean regions. Nevertheless, our results further highlight the apparently larger magnitude of ST forcing over AS and ST response over BOB and SCS, compared to the ST response over AS and the ST forcing over BOB and SCS, respectively. The results also imply comparable magnitudes of the land–air interaction over IP and the sea–air interactions over BOB and SCS. Over ICP and SC, the TCCs between rainfall and ST are always small (Figs. 8e and 8f), suggesting relatively weaker land–air interaction over these two regions.

The CFSv2 forecasts reasonably capture the observed transitions of the local ST–rainfall relationship over the various regions. However, the simultaneous positive correlation over AS is apparently overestimated in the long-lead forecasts and the correlation is even higher

than the correlation between rainfall and the 1-pentad lead ST (Fig. 8a), indicating quicker- and stronger-than-observed influences of ST on local rainfall in long lead predictions. Meanwhile, the negative correlations between rainfall and 1-pentad lagged ST are underestimated in the long-lead forecasts over BOB and in all-lead forecasts over SCS (Figs. 8b and 8c). Over IP and ICP where the closest connection is observed when the ST lags the rainfall by 1 pentad, simultaneous negative correlations are mostly significant and are exaggerated by forecasts of various leads, denoting quicker- and stronger-than-observed responses of land ST to rainfall in the model (Figs. 8d and 8e).

Given that the strongest relationships between regional ST and rainfall often appear when the former leads or lags the latter by 1–2 pentads, we further analyze the TCCs between ST and rainfall in different years, for a 1-pentad ST lead and lag (Fig. 9). Observations show apparent regional differences in ST–rainfall relationship on the subseasonal scale. Over AS, the TCCs at a 1-pentad ST lead are positive in all years, with an average above the 95% confidence level. From a 1-pentad lead to a 1-pentad lag, changes from positive correlations to weak negative correlations only appear in one-third of the years, showing that ST response is mostly slow and weak compared to ST forcing. In contrast, over BOB and SCS, most positive correlations at a 1-pentad ST lead change into significant negative correlations at a 1-pentad ST lag, suggesting that the sea–air interactions over BOB and SCS are typically characterized by ST forcing on the atmosphere first and the atmosphere feedbacks onto ST afterward. Over land, positive correlations at a 1-pentad ST lead are always observed with only a few exceptions. At a 1-pentad ST lag, negative and mostly significant correlations are found over IP, while the correlations over ICP and SC are mostly negative but insignificant. This feature once again proves that, although characterized by processes of ST forcing and atmospheric feedback, land–air interactions are overall weak except over IP, where a magnitude of interaction comparable to that over BOB and SCS is found and the response of ST to local rainfall is especially remarkable.

Although with reasonable skill, the forecast results given in Fig. 9 show again the overestimated ocean–atmosphere effect over AS and the underestimated atmosphere–ocean effect over BOB and SCS in long-lead predictions. Also, significant interannual differences in lagged ST–rainfall relationships and intense fluctuations of the relationships with lead time are found over various regions. Furthermore, the interannual differences of forecast skill of regional rainfall are associated with the obvious disparities in local ST–rainfall relationships. For the forecasts of rainfall over AS in 1999 and 2007, for example, the low TCCs and their quick decreases with lead time [Fig. 5a(1)] clearly denote unskillful forecasts of the rainfall. Correspondingly, the predictions exhibit intense fluctuations of ST–rainfall relationships with lead time [Figs. 9a(1) and 9b(1)]. Similar features are also seen in 2010 for forecasts of the rainfall over both BOB and SCS [Figs. 5a(2) and 5a(3) and Figs. 9a(2), 9a(3), 9b(2), and 9b(3)]. In contrast, the forecasts of AS rainfall in 2000 and 2006 and BOB rainfall in 1999 and 2007 show high and slowly dropping TCCs along with relatively stable variations of ST–rainfall relationships with lead time. Of course, the differences in connection between regional rainfall and ST are often coupled with different distributions of extensive anomalies of ST and large-scale circulation. The above results imply that, to some extent, the apparent differences in local ST–rainfall relationships may contribute to the disparities of predictability of regional rainfall.

6. Modulation of BSISO

In boreal summer, BSISO prevails over the ASM region and modulates the variability of regional rainfall. Here we explore the skill of BSISO forecast, interannual differences of BSISO, and their relationships with forecasts of regional rainfall.

Lee et al. (2013) proposed two real-time BSISO indices based on a multivariate empirical orthogonal function (EOF) analysis of the daily 850-hPa zonal wind and OLR over 10°S–40°N, 40°–160°E. The BSISO1, defined by the first two principal components (PCs), represents the canonical northward-propagating intraseasonal oscillation (ISO) with periods of 30–60 days. The BSISO2, defined by the third and fourth PCs, describes the northward- and northwestward-propagating ISO with periods of 10–30 days. In this study, we employ the same procedure as Lee et al. (2013) to derive the observed BSISO1 and BSISO2 indices using the daily series of CFSR wind and NOAA OLR. Similar EOF modes and phase cycles of BSISO to the previously shown are obtained. Hindcasted BSISO indices are also computed by projecting the combined anomaly fields onto the observed modes.

Figure 10 shows the forecast skill of BSISO1 and BSISO2 based on bivariate anomaly correlation (BAC) and RMSE as defined by Lin et al. (2008). For the overall BAC skill from June to September during 1999–2010, taking 0.5 as the threshold of useful skill, the BSISO1 and BSISO2 can be predicted in advance by 12 and 9 days, respectively. Obvious interannual differences, featured by a minimum of 8 days in 2010 and a maximum of 17 days in 2008 for BSISO1, as well as a minimum of 8 days in 2003 and 2006 and a maximum of

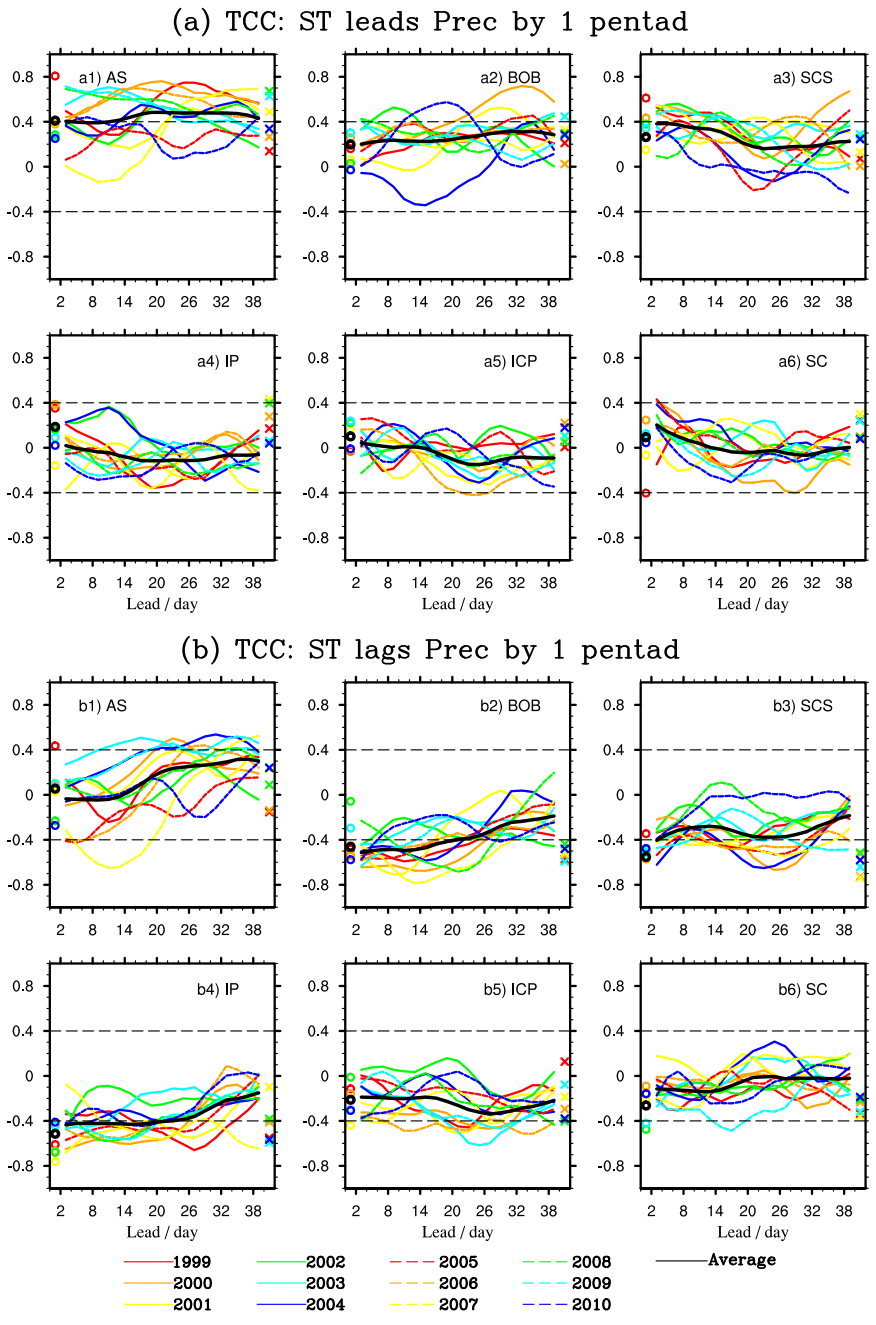

FIG. 9. As in Fig. 8, but multiyear-averaged lagged correlations are replaced by correlations of rainfall with surface temperature of (a) 1-pentad lead and (b) 1-pentad lag in each year.

12 days in 2010 for BSISO2, are also found (Figs. 10a and 10b). When measured by RMSE, different interannual variations of forecast skill are shown, but overall the same useful skill as BACs are found for all forecast cases (Figs. 10c and 10d). The performance of forecast of intraseasonal oscillation is often dependent on the amplitude of the oscillation. For the BSISO1 BAC averaged over 0–10 lead days, its correlation with the amplitude of observed BSISO1 $[(PC1^2 + PC2^2)^{1/2}]$ on an interannual time scale is as high as 0.86. For BSISO2, however, the correlation between BAC and $(PC3^2 + PC4^2)^{1/2}$ is only 0.44, which is below the 90% confidence level. It is also seen from Fig. 10e that the interannual variation of BSISO2 amplitude is more poorly captured by the model, characterized by a quick decrease in skill with lead time, compared to BSISO1. The above result

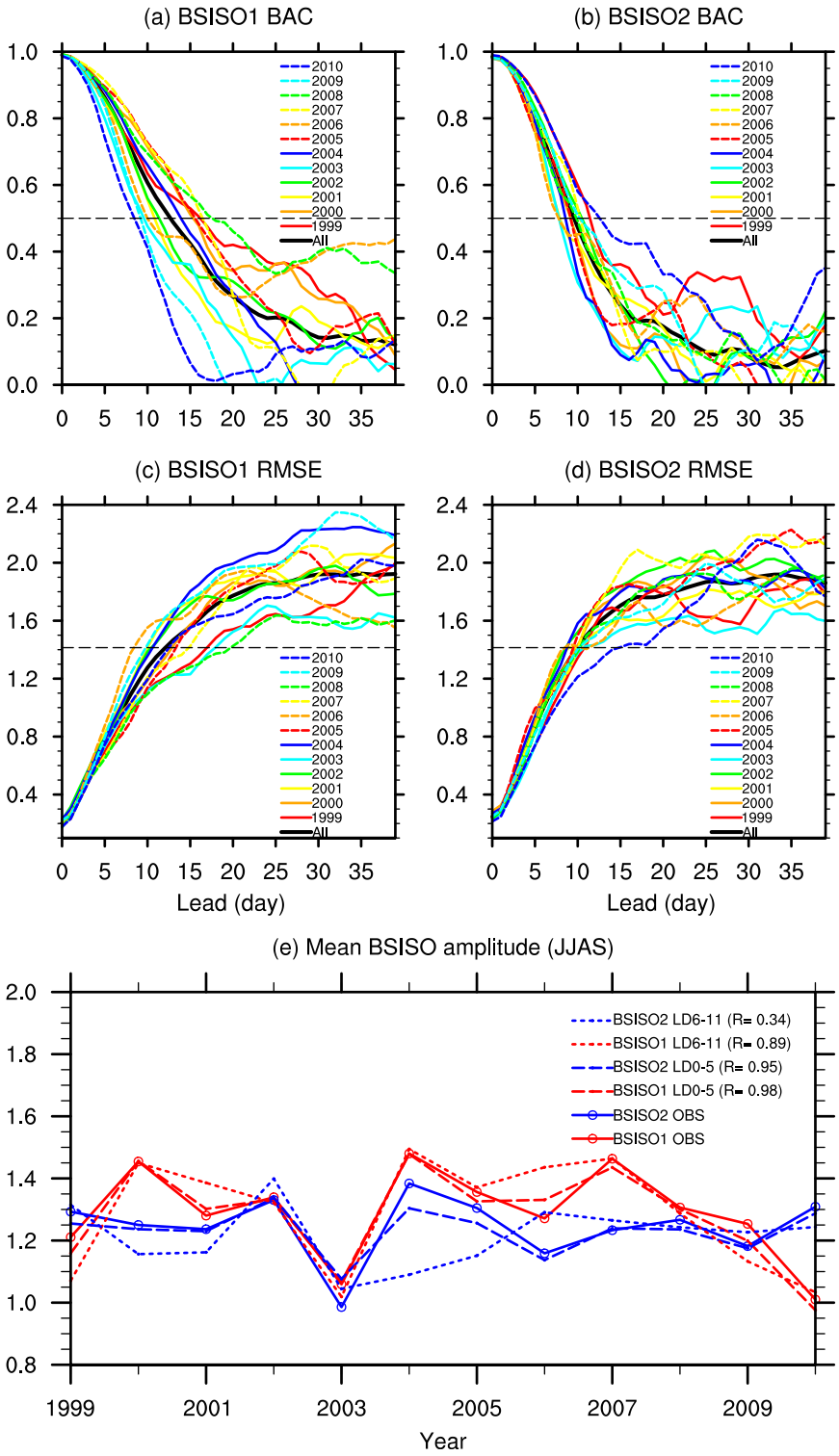

FIG. 10. Bivariate (a),(b) anomaly correlations and (c),(d) root-mean-square errors between observations and forecasts as a function of lead time for (a),(c) BSISO1 and (b),(d) BSISO2 during June–September in each year from 1999 to 2010. Shown are also (e) interannual variations of amplitude of BSISO1 and BSISO2 in observations and forecasts of 0–5 lead days and 6–11 lead days. The black dashed horizontal lines represent 0.5 in (a),(b) and 1.414 in (c),(d), and the decimal values in parentheses shown in (e) are the temporal correlations between forecasts and observations.

suggests that it is more difficult in forecasting BSISO2 than forecasting BSISO1. Compared to the result given in Fig. 5a, in terms of the mean skill for 0–10 lead days, the correlations between forecast skill for regional rainfall and BSISO are mostly insignificant, except between BOB or SCS rainfall and BSISO1 ($R = 0.56$), and between IP rainfall and BSISO2 ($R = 0.62$). (The threshold value of the 90% confidence level is 0.50 and that of the 95% confidence level is 0.58.) In 2009 and 2010 when BSISO1 is poorly predicted, the forecasts of rainfall over BOB and SCS show quickly decreasing skill. Also in 2003 when both BSISO1 and BSISO2 are poorly captured, the forecasts of rainfall over SCS and IP exhibit rapid decreases in skill with lead time (Figs. 10 and 5). In addition, the correlation between forecast skill for SC or ICP rainfall and BSISO1 is −0.49, a value close to the 90% confidence level. The above result indicates that, certain factors may commonly affect the forecasts of BSISO and regional rainfall, although the predictability of large-scale circulation and regional rainfall is often attributed to different aspects.

Given the dependence of forecast skill of BSISO on the target phase, we further show the BACs of BSISO1 and BSISO2 as a function of target phase and lead time (Fig. 11). For each phase, BACs are computed for target days when the phase angle of observed BSISO is within the particular phase and the amplitude of BSISO is greater than 1. Significant variations of skill with the target phase are found for lead times longer than one week, with relatively low BACs in phases 4 and 8 for BSISO1 and phases 1 and 5 for BSISO2. The low skill for

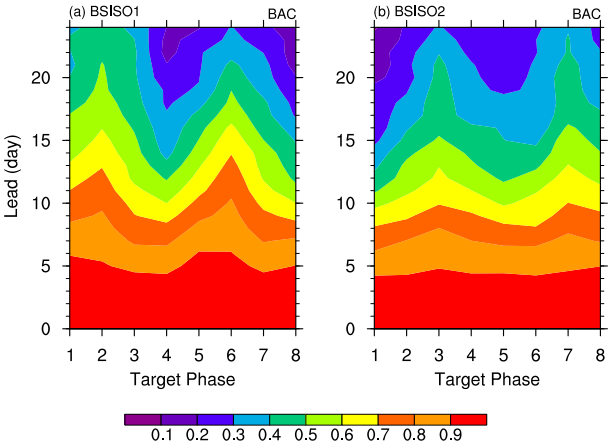

FIG. 11. Bivariate anomaly correlations between observations and forecasts as a function of lead time and target phase of (a) BSISO1 and (b) BSISO2.

target phases 4 and 8 of BSISO1 implies that the model has difficulty in forecasting the propagation of BSISO1 across BOB, MC, and the western North Pacific. It is also suggested that long lead forecasts are less skillful in capturing the initiation of BSISO2 over the equatorial eastern Indian Ocean and the Philippine Sea as well as the propagation of BSISO2 from the western North Pacific to East Asia. Figure 12 shows the observed features of mean amplitude and occurrence frequency from June to September for each of the eight phases. In 2003 and 2010 when low forecast skill for BSISO1 are found, BSISO1 activity is concentrated near phase 4, which is hard to predict. In contrast, the better predictions of

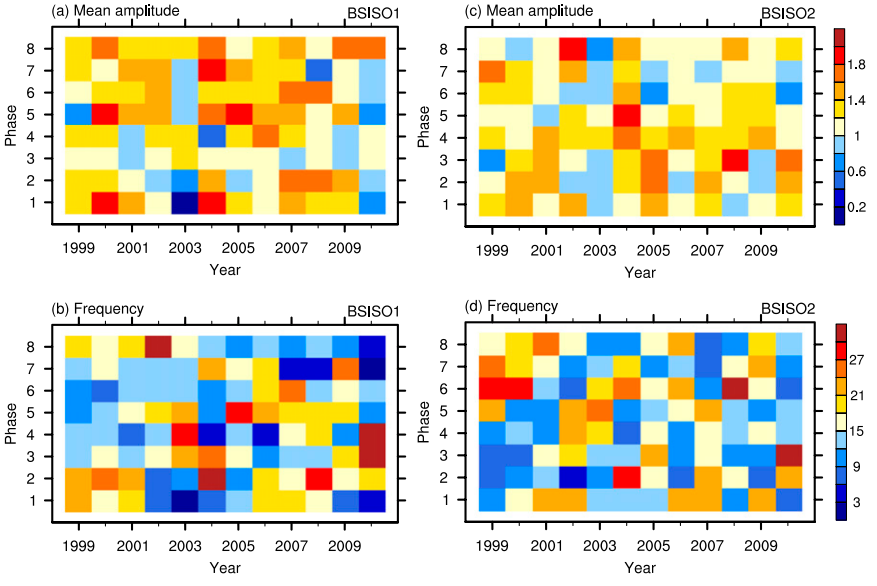

FIG. 12. The observed (a),(c) mean amplitude and (b),(d) occurrence frequency (day) for the eight phases of (left) BSISO1 and (right) BSISO2 during June–September in each year.

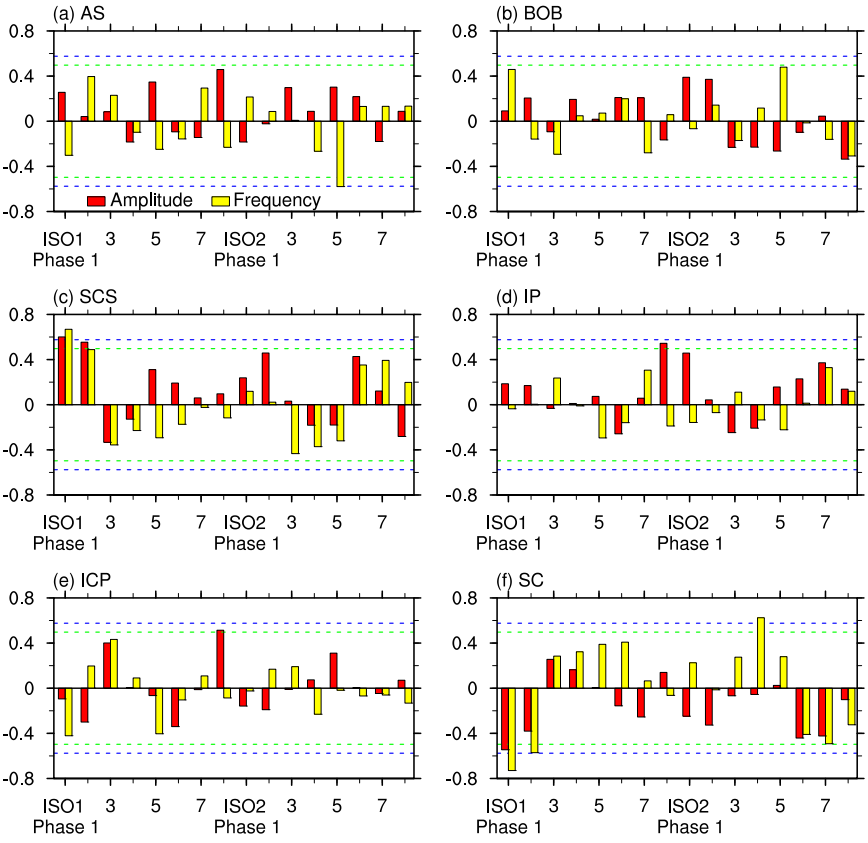

FIG. 13. Interannual correlations between forecast skill (averaged over 0–10 lead days) of regionally averaged rainfall and observed phases of BSISO1 and BSISO2. The red and yellow bars represent the mean amplitude and frequency of BSISO phases, and the green and blue dashed lines denote the values of statistical significance at the 90% and 95% confidence level, respectively.

BSISO1 in 2007 and 2008 are associated with the more frequent occurrence of BSISO1 near phase 2 or 6, which is easier to forecast. Similarly, comparisons between the unskillful cases in 2003 and 2006 and the skillful cases in 1999 and 2010 for BSISO2 also indicate more predictable phases for the former and more unpredictable phases for the latter. This result suggests that apparent interannual differences of BSISO forecast skill are always featured by drifts of the observed BSISO phase toward the most predictable or unpredictable mode in addition to the changes in mean amplitude, which may further provide a modulation on the characteristics of rainfall and its forecast.

Figure 13 shows the interannual relationships between the forecast skill of regional rainfall and the observed mean amplitude and frequency of BSISO phases. The frequency and/or amplitude of phases 1 and 2 of BSISO1 are significantly and positively correlated with the forecast skill of SCS rainfall but negatively correlated with that of SC rainfall. Given that the subseasonal variations of SCS and SC rainfall are anticorrelated in both observations and predictions (figure not shown), this feature means notable modulations of BSISO1 on the forecasts of rainfall over these two regions, which are obviously out of phase. When BSISO1 phases 1 and 2 show more frequent occurrence or larger amplitude in summer (i.e., large convection suppression over SCS and small convection enhancement over SC), subseasonal forecasts are often skillful for SCS rainfall and unskillful for SC rainfall, and vice versa. In this case, it is also easy to predict BSISO1 (Fig. 11a) and why BSISO1 BACs are positively correlated with the forecast skill of SCS rainfall but negatively correlated with the forecast skill of SC rainfall is thus partially explained. For BSISO2, significant relationships between the frequency of phase 5 and the forecast of AS rainfall, as well as between the frequency of phase 4 and the forecast of SC rainfall, are also found, but without significant relationships between the corresponding phase amplitude and the forecast of regional rainfall. Besides, most of other correlations are below the 95% confidence level. This feature is because the forecast of regional rainfall is comprehensively

influenced by all phases of the BSISO cycle and its linear relationship with a certain phase is overall limited. It is also because the model may be incapable of fully reproducing the realistic modulation due to its limitations in capturing the variability of BSISO, regional rainfall, and their relationships.

7. Summary and discussion

We have investigated the subseasonal predictions of regional summer monsoon rainfall over tropical Asian land and oceans by analyzing the hindcasts of the NCEP CFSv2. The model shows reasonable skill and apparent regional differences for rainfall over the various ASM regions. Overall, higher PCCs between forecasts and observations, and more remarkable interannual differences in skill, are found over oceans than over land, with the longest lead of skillful predictions over AS (about 9 days on average) and the shortest over ICP (only 0 day on average). The TCCs also show a slower decrease with lead time for forecasts over oceans than over land, and the averaged lead time for TCCs to become unskillful is beyond 11 days over AS and 1 day over ICP. This actual forecast skill is far lower than the potential forecast skill, which is often useful at a lead time above 40 days over oceans and about 2–3 weeks over land. In particular, the largest and smallest ratios of potential skill to actual skill are found over ICP and SC, respectively. TCCs and PCCs of rainfall do not show significant linear relationships, but they present relatively close connections with forecast skill in ST. Especially, apparently close linear relationships between the PCCs of rainfall and ST are often found over most regions except BOB.

In observation, the local rainfall–ST correlation over AS attains a significant positive maximum at a 1-pentad ST lead and becomes weak negative values at the ST lags of 2 pentads or more. Over BOB, SCS, and IP, the strongest positive and negative correlations appear at a 2-pentad ST lead and a 1-pentad ST lag, respectively, and the latter is especially notable. Over ICP and SC, although a change in local rainfall–ST relationships from positive at a 1-pentad ST lead to negative at a 1-pentad ST lag is also found, correlations are often small and insignificant. These features suggest apparent differences in the underlying surface–air interaction process among the various regions, and in the interaction between oceans and land. The CFSv2 forecasts reasonably capture the observed transitions of local rainfall–ST relationship with a lag time over the various regions. However, they also exhibit evident deficiencies, including an overestimation of the simultaneous positive correlations over AS in long-lead forecasts, an underestimation of the negative correlations at a 1-pentad ST lag over BOB in long-lead forecasts and over SCS in all-lead forecasts, and an exaggeration of the simultaneous negative correlations over IP and ICP in predictions of all leads. To some extent, these results reveal the model's inability in reproducing the forcing and response of the underlying surface temperature and atmosphere over different regions. Furthermore, the ST–rainfall relationships in predictions show significant interannual differences, which fluctuate with lead time and are sometimes associated with apparent interannual disparities in forecast skill of regional rainfall. In addition, in observations local rainfall is often significantly related to regional circulation, while in forecasts it shows a gradually intensifying connection with large-scale circulation and ST over extensive regions as lead time increases. In particular, in long-lead forecasts the connection between rainfall over BOB and SCS is remarkably strengthened and their regional differences in relationships with large-scale features are hardly distinguishable.

The modulation of BSISO on forecast of regional rainfall is also explored. More remarkable interannual differences in forecast skill and amplitude, as well as more significant relationship between the two, are often found in BSISO1 compared to BSISO2. Although the interannual relationships between forecast skill of BSISO and regional rainfall are mostly insignificant, reasonable correlations between the forecasts of BSISO1 and BOB or SCS rainfall, and between the forecasts of BSISO2 and IP rainfall, are still found, suggesting the possible connections between the predictions of large-scale features and the local characteristics over certain regions. It is further shown that apparent interannual differences in the forecast skill of BSISO are always featured by drifts of observed BSISO phase toward the most predictable or unpredictable mode, in addition to the change in the mean amplitude of BSISO, which may thus modulate the forecast of regional rainfall. Then, reasonable interannual relationships between the forecast skill of regional rainfall and observed mean amplitude and frequency of BSISO phases can be obtained. In particular, BSISO1 phases 1–2 are significantly and positively correlated to the forecast skill of SCS rainfall but negatively correlated to that of SC rainfall, implying notable modulations of BSISO1 on the forecasts of regional rainfall and out-of-phase impacts between the two regions.

The above findings are helpful for further understanding the discrepancies of rainfall predictability among the various ocean and land domains. Less predictable rainfall is often found over land than over oceans, which should be mainly attributed to the localized connection of land rainfall with atmospheric circulation and the weak local land–air interaction. Indeed, these two aspects are

closely interrelated to each other. Insignificant local ST–rainfall relationships over land are adverse to destabilizing the atmosphere and producing heavy convective rainfall, thus further inducing large-scale circulation anomalies. On the other hand, without a support from large-scale anomalies, a strong local land–air interaction cannot last for too long. Of course, in addition to the characteristics of land rainfall itself, a model's deficiencies, especially the overestimation of the simultaneous local rainfall–ST relationships and the gradually strengthening connections among neighboring regions with increasing lead time, are also important influential factors. Among the three land regions, the rainfall over ICP has the lowest forecast skill because it severely suffers from the limitations discussed above. By comparison, the rainfall over IP is often related to relatively extensive circulation anomalies (figure not shown) and it interacts with local ST in a magnitude comparable to the rainfall over BOB and SCS, although in models the simultaneous local rainfall–ST relationship over IP is significantly exaggerated as compared to that over ICP. Although characterized by local features and weak land–air interaction that are difficult to predict, the model does not show an apparent overestimation for the rainfall over SC, and the forecast of SC rainfall is significantly modulated by phases 1–2 of BSISO1. This may to some extent contribute to the reasonable performance of the actual forecast of SC rainfall compared to its potential forecast skill.

Over the ocean domains, CFSv2 also shows obvious deficiencies in describing the relationships of regional rainfall with local ST, large-scale circulation, and the rainfall over other regions. However, ocean rainfall itself is related to more extensive circulation and affected by stronger sea–air interaction, denoting more predictable features. The variability of AS rainfall is clearly different from that of BOB and SCS rainfall. On the one hand, the former is more attributed to the northward extension of cross-equatorial flow from Somali and its regional feature is captured by forecasts of various leads. However, the latter is more attributed to the zonal wind over the southern ASM region and its regional characteristic in forecasts becomes gradually indistinguishable as lead time increases. On the other hand, the former is featured by a strong and quick ocean–atmosphere effect but a weak and slow atmosphere–ocean effect, while the latter is represented by relatively weaker and slower SST forcing but an obviously stronger and faster SST response, although both the forcing and response encounter varying degrees of distortion in CFSv2 forecasts. These differences may largely contribute to the larger predictability of the rainfall over AS compared to the rainfall over BOB and SCS. Roxy et al. (2013) noticed the strong and fast SST forcing over AS, ascribing it to the presence of a large zonal gradient of SST, but did not stress the weak local SST response. The weaker response of AS SST than its forcing suggests that the subseasonal SST variability over AS is less affected by local and rapidly varying atmospheric feedback compared to that over the other oceans, which may, along with the impact of large-scale circulation, contribute to the high predictability of the AS SST (Fig. 5b). Then, the more predictable SST and its strong forcing on the atmosphere may lead to the higher forecast skill of rainfall over AS (Fig. 5a), although the degree to which the two are interrelated is different from one year to another. The close connection between the rainfall over BOB and SCS and their similar relationships with other factors are unrealistically shown in the model, and their forecast skill is related to the ability of BSISO1 forecast, partially resulting in similar forecast skill for those two regions.

Inclusion of sea/land–air coupling plays an important role in the simulation and prediction of subseasonal climate variability (e.g., Waliser et al. 1999; Pegion and Kirtman 2008; Fu et al. 2008, 2013a). Unfortunately, forecast models themselves possess limited capability of capturing the regional characteristics of this coupling because the predictable signals tend to be dominated by the variations of slowly varying components in association with large-scale coupling features as the lead time increases (Liu et al. 2014a). Thus, the subseasonal forecast skill of regional rainfall is often limited and it suffers from the impact of unrealistic local sea–land–air interaction as shown in the current study. Albeit with such limitation, further work on correcting erroneous surface–atmosphere interaction is much needed. For example, for the model diagnosed in this study, the exaggeratedly fast and strong ST responses to atmosphere variability over IP and ICP need to be rectified.

Owing to its unique geographical location and complex distributions of land, sea, and terrains, the Maritime Continent induces complex and intense variations of convection on various time and space scales. It serves as a ''boiler box'' of the tropics (Ramage 1968) and affects the climate in and outside the region significantly (Neale and Slingo 2003; Jiang et al. 2013b). Recently, Zhang et al. (2015) carried out a detailed analysis of the seasonal prediction of MC rainfall by the NCEP CFSv2 for wet and dry seasons, focusing on the influences of ENSO and large-scale monsoon circulation. As a supplementary analysis, we also examine the skill of subseasonal forecast of MC rainfall by CFSv2. Figure 14 shows the prediction skill of rainfall and ST over 10°S–10°N, 95°–145°E. The PCCs of rainfall and ST overall present inconspicuous interannual variations, and they are often useful for long lead forecasts with a lead time

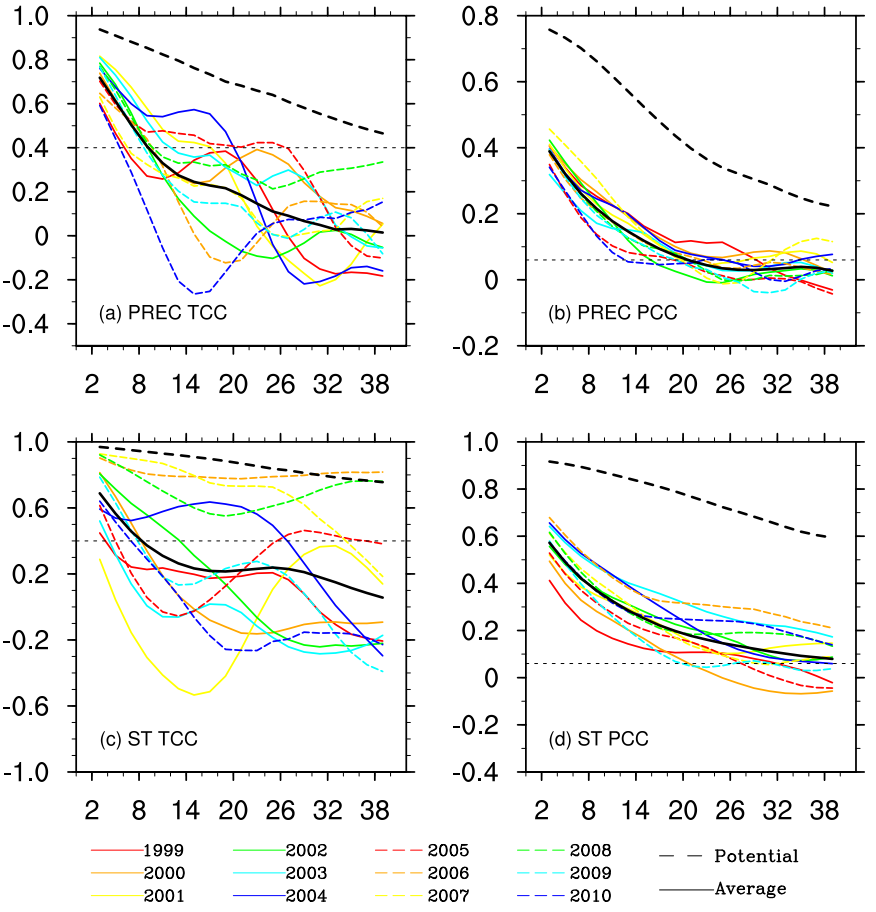

FIG. 14. (left) As in Fig. 5, but for the temporal correlations of (a) rainfall and (c) surface temperature over the Maritime Continent. (right) As in Fig. 4b, but for the spatial pattern correlations of (b) rainfall and (d) surface temperature over the Maritime Continent.

above three weeks. In contrast, the TCCs of both rainfall and ST show a quicker drop with the increasing lead time, and become insignificant near the 9-day lead on average. Remarkable interannual differences of TCCs are also found, but with insignificant correlations between the forecasts of rainfall and ST. The unskillful forecasts of the temporal variability of rainfall and temperature may be partially attributed to the unrealistic local ST–rainfall relationships in the model. It is also seen that weak ocean–atmosphere and atmosphere–ocean effects in observations are nearly replaced by overestimated and one-sided ocean–atmosphere impact in most forecasts except at a short lead time (Fig. 15). This feature indicates that the regional atmospheric response to ST forcing over MC is often quickly exaggerated as lead time increases.

The performance in predicting MC rainfall may account for the usefulness of rainfall forecast over other regions. With respect to the average skill of forecasts within 5-, 10-, and 15-day time leads, interannual variations of the TCC over MC overall show insignificant correlations with those over the various domains analyzed in this study except for IP, as well as with BSISO1 BACs. However, it has been pointed out that BSISO1 is most unskillfully predicted when it propagates across MC. Indeed Wang et al. (2014) also showed the difficulty of CFSv2 in forecasting the eastward propagation of the Madden–Julian oscillation across the MC. This feature may be related to the model's inability in capturing the response of regional convection to ST forcing. Given the important modulation of large-scale intraseasonal oscillation on regional monsoon rainfall, the forecast of rainfall over MC undoubtedly influences the predictions of BSISO1 and the Madden–Julian oscillation and furthers the forecast of rainfall over other regions.

It is also interesting to note the significant negative correlation between the forecasts of rainfall over MC and IP ($R = -0.58$). It is argued that the feature may be related to the influence of BSISO2 forecast, which is

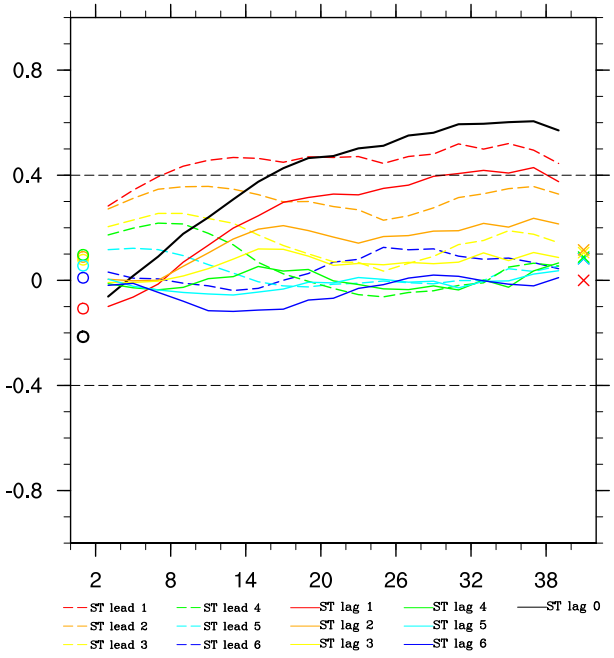

FIG. 15. Multiyear-averaged temporal correlations of regional average rainfall with surface temperature of 6-pentad lead to 6-pentad lag over the Maritime Continent. Curves show the variations of forecasts with lead time, and open circles and crosses (only refer to the *y* coordinate) denote the observations corresponding to the same-color solid lines and dashed lines, respectively. Shown are the three-point running averages along forecast lead days, and black dashed horizontal lines denote the values of statistical significance of correlation at the 95% confidence level.

negatively correlated with the forecast of MC rainfall ($R = -0.86$) but positively correlated with the forecast of IP rainfall ($R = 0.62$; refer to section 6). The multiyear mean regressions of 850-hPa winds on averaged rainfall over MC show that, on the subseasonal scale, the anomalous MC rainfall is associated with a significant zonal wind response over the southern SCS and the Philippine Sea (figure not shown). This circulation pattern tends to appear in BSISO2's phase 5 and is not easily seen in BSISO2's phases 3 and 7, in which cyclonic or anticyclonic wind anomalies dominate over the Southeast Asian monsoon region and thus notable meridional wind anomalies prevail near the Philippine Sea. This feature suggests that, when skillful forecasts of MC rainfall often realistically reproduce the relationships between regional rainfall and large-scale circulation, BSISO2 often prefers to stay at the most unpredictable phases rather than the most predictable phases in the model (refer to Fig. 11), thus contributing to an anticorrelation between the forecasts of MC rainfall and BSISO2. Then, MC rainfall prediction may affect the forecasts of rainfall over other regions in which BSISO2 serves as a bridge. The above results only imply the interregional influence of MC rainfall forecast, and future in-depth studies are needed to reveal the underlying physical processes.

Acknowledgments. The authors thank the four anonymous reviewers for their fruitful suggestions that were helpful in improving the overall quality of the manuscript. This study was jointly supported by the National Basic Research Program of China (Grants 2015CB453200 and 2014CB953900), the National Natural Science Foundation of China (Grants 41305057, 41275076, and 41375081), Guangdong Province Funds for China National "Thousand-Talent Plan" (YCJ2013-196), and the LASW State Key Laboratory Special Fund (2013LASW-A05).

REFERENCES

Abhilash, S., and Coauthors, 2014: Prediction and monitoring of monsoon intraseasonal oscillations over Indian monsoon region in an ensemble prediction system using CFSv2. *Climate Dyn.*, **42**, 2801–2815, doi:10.1007/s00382-013-2045-9.

Arakawa, O., and A. Kitoh, 2004: Comparison of local precipitation–SST relationship between the observation and a reanalysis dataset. *Geophys. Res. Lett.*, **31**, L12206, doi:10.1029/2004GL020283.

Arribas, A., and Coauthors, 2011: The GloSea4 ensemble prediction system for seasonal forecasting. *Mon. Wea. Rev.*, **139**, 1891–1910, doi:10.1175/2010MWR3615.1.

Drbohlav, H.-K. L., and V. Krishnamurthy, 2010: Spatial structure, forecast errors, and predictability of the South Asian monsoon in CFS monthly retrospective forecasts. *J. Climate*, **23**, 4750–4769, doi:10.1175/2010JCLI2356.1.

Fu, X., B. Wang, T. Li, and J. P. McCreary, 2003: Coupling between northward-propagating intraseasonal oscillations and sea surface temperature in the Indian Ocean. *J. Atmos. Sci.*, **60**, 1733–1753, doi:10.1175/1520-0469(2003)060<1733:CBNIOA>2.0.CO;2.

——, B. Yang, Q. Bao, and B. Wang, 2008: Sea surface temperature feedback extends the predictability of tropical intraseasonal oscillation. *Mon. Wea. Rev.*, **136**, 577–597, doi:10.1175/2007MWR2172.1.

——, B. Wang, Q. Bao, P. Liu, and J.-Y. Lee, 2009: Impacts of initial conditions on monsoon intraseasonal forecasting. *Geophys. Res. Lett.*, **36**, L08801, doi:10.1029/2009GL037166.

——, ——, J.-Y. Lee, W. Wang, and L. Gao, 2011: Sensitivity of dynamical intraseasonal prediction skills to different initial conditions. *Mon. Wea. Rev.*, **139**, 2572–2592, doi:10.1175/2011MWR3584.1.

——, J.-Y. Lee, P. Hsu, H. Taniguchi, B. Wang, W. Wang, and S. Weaver, 2013a: Multi-model MJO forecasting during DYNAMO/CINDY period. *Climate Dyn.*, **41**, 1067–1081, doi:10.1007/s00382-013-1859-9.

——, ——, B. Wang, W. Wang, and F. Vitart, 2013b: Intraseasonal forecasting of the Asian summer monsoon in four operational and research models. *J. Climate*, **26**, 4186–4203, doi:10.1175/JCLI-D-12-00252.1.

Hendon, H. H., and J. Glick, 1997: Intraseasonal air–sea interaction in the tropical Indian and Pacific Oceans. *J. Climate*, **10**, 647–661, doi:10.1175/1520-0442(1997)010<0647:IASIIT>2.0.CO;2.

Huffman, G. J., R. F. Adler, M. Morrissey, D. T. Bolvin, S. Curtis, R. Joyce, B. McGavock, and J. Susskind, 2001: Global precipitation at one-degree daily resolution from multisatellite observations. *J. Hydrometeor.*, **2**, 36–50, doi:10.1175/1525-7541(2001)002<0036:GPAODD>2.0.CO;2.

Jiang, X., S. Yang, Y. Li, A. Kumar, X. Liu, Z. Zuo, and B. Jha, 2013a: Seasonal-to-interannual prediction of the Asian summer monsoon in the NCEP Climate Forecast System version 2. *J. Climate*, **26**, 3708–3727, doi:10.1175/JCLI-D-12-00437.1.

——, ——, ——, ——, W. Wang, and Z. Gao, 2013b: Dynamical prediction of the East Asian winter monsoon by the NCEP Climate Forecast System. *J. Geophys. Res. Atmos.*, **118**, 1312–1328, doi:10.1002/jgrd.50193.

Joseph, S., A. K. Sahai, and B. N. Goswami, 2010: Boreal summer intraseasonal oscillations and seasonal Indian monsoon prediction in DEMETER coupled models. *Climate Dyn.*, **35**, 651–667, doi:10.1007/s00382-009-0635-3.

Kang, H., C. K. Park, S. Hameed, and K. Ashok, 2009: Statistical downscaling of precipitation in Korea using multimodel output variables as predictors. *Mon. Wea. Rev.*, **137**, 1928–1938, doi:10.1175/2008MWR2706.1.

Kim, H. M., I. S. Kang, B. Wang, and J. Y. Lee, 2008: Interannual variations of the boreal summer intraseasonal variability predicted by ten atmosphere–ocean coupled models. *Climate Dyn.*, **30**, 485–496, doi:10.1007/s00382-007-0292-3.

——, P. J. Webster, J. A. Curry, and V. E. Toma, 2012: Asian summer monsoon prediction in ECMWF System 4 and NCEP CFSv2 retrospective seasonal forecasts. *Climate Dyn.*, **39**, 2975–2991, doi:10.1007/s00382-012-1470-5.

Kirtman, B., and Coauthors, 2014: The North American Multimodel Ensemble: Phase-1 seasonal-to-interannual prediction; phase-2 toward developing intraseasonal prediction. *Bull. Amer. Meteor. Soc.*, **95**, 585–601, doi:10.1175/BAMS-D-12-00050.1.

Krishna Kumar, K., M. Hoerling, and B. Rajagopalan, 2005: Advancing dynamical prediction of Indian monsoon rainfall. *Geophys. Res. Lett.*, **32**, L08704, doi:10.1029/2004GL021979.

Lee, J. Y., and Coauthors, 2010: How are seasonal prediction skills related to models' performance on mean state and annual cycle? *Climate Dyn.*, **35**, 267–283, doi:10.1007/s00382-010-0857-4.

——, B. Wang, M. Wheeler, X. Fu, D. Waliser, and I. Kang, 2013: Real-time multivariate indices for the boreal summer intraseasonal oscillation over the Asian summer monsoon region. *Climate Dyn.*, **40**, 493–509, doi:10.1007/s00382-012-1544-4.

Liebmann, B., and C. A. Smith, 1996: Description of a complete (interpolated) outgoing longwave radiation dataset. *Bull. Amer. Meteor. Soc.*, **77**, 1275–1277.

Lin, H., G. Brunet, and J. Derome, 2008: Forecast skill of the Madden–Julian oscillation in two Canadian atmospheric models. *Mon. Wea. Rev.*, **136**, 4130–4149, doi:10.1175/2008MWR2459.1.

Liu, X., S. Yang, A. Kumar, S. Weaver, and X. W. Jiang, 2013: Diagnostics of subseasonal prediction biases of the Asian summer monsoon by the NCEP Climate Forecast System. *Climate Dyn.*, **41**, 1453–1474, doi:10.1007/s00382-012-1553-3.

——, ——, Q. Li, A. Kumar, S. Weaver, and S. Liu, 2014a: Subseasonal forecast skills and biases of global summer monsoons in the NCEP Climate Forecast System version 2. *Climate Dyn.*, **42**, 1487–1508, doi:10.1007/s00382-013-1831-8.

——, and Coauthors, 2014b: Relationships between interannual and intraseasonal variations of the Asian-western Pacific summer monsoon hindcasted by BCC_CSM1.1(m). *Adv. Atmos. Sci.*, **31**, 1051–1064, doi:10.1007/s00376-014-3192-6.

——, T. Wu, S. Yang, W. Jie, S. Nie, Q. Li, Y. Cheng, and X. Liang, 2015: Performance of the seasonal forecasting of the Asian summer monsoon by BCC_CSM1.1(m). *Adv. Atmos. Sci.*, **32**, 1156–1172, doi:10.1007/s00376-015-4194-8.

Molteni, F., and Coauthors, 2011: The new ECMWF seasonal forecast system (System 4). ECMWF Tech. Memo. 656, ECMWF, 49 pp.

Neale, R., and J. Slingo, 2003: The Maritime Continent and its role in the global climate: A GCM study. *J. Climate*, **16**, 834–848, doi:10.1175/1520-0442(2003)016<0834:TMCAIR>2.0.CO;2.

Neena, J. M., J.-Y. Lee, D. Waliser, B. Wang, and X. Jiang, 2014: Predictability of the Madden–Julian oscillation in the Intraseasonal Variability Hindcast Experiment (ISVHE). *J. Climate*, **27**, 4531–4543, doi:10.1175/JCLI-D-13-00624.1.

Pegion, K., and B. P. Kirtman, 2008: The impact of air–sea interactions on the simulation of tropical intraseasonal variability. *J. Climate*, **21**, 6616–6635, doi:10.1175/2008JCLI2180.1.

——, and P. D. Sardeshmukh, 2011: Prospects for improving subseasonal predictions. *Mon. Wea. Rev.*, **139**, 3648–3666, doi:10.1175/MWR-D-11-00004.1.

Pope, V., and R. Stratton, 2002: The processes governing horizontal resolution sensitivity in a climate model. *Climate Dyn.*, **19**, 211–236, doi:10.1007/s00382-001-0222-8.

Preethi, B., R. H. Kripalani, and K. K. Krishna, 2010: Indian summer monsoon rainfall variability in global ocean-atmospheric models. *Climate Dyn.*, **35**, 1521–1533, doi:10.1007/s00382-009-0657-x.

Rajeevan, M., C. K. Unnikrishnan, and B. Preethi, 2012: Evaluation of the ENSEMBLES multi-model seasonal forecasts of Indian summer monsoon variability. *Climate Dyn.*, **38**, 2257–2274, doi:10.1007/s00382-011-1061-x.

Ramage, C. S., 1968: Role of a tropical "Maritime Continent" in the atmospheric circulation. *Mon. Wea. Rev.*, **96**, 365–369, doi:10.1175/1520-0493(1968)096<0365:ROATMC>2.0.CO;2.

Reichler, T., and J. O. Roads, 2005: Long-range predictability in the tropics. Part II: 30–60-day variability. *J. Climate*, **18**, 634–650, doi:10.1175/JCLI-3295.1.

Roxy, M., and Y. Tanimoto, 2007: Role of SST over the Indian Ocean in influencing the intraseasonal variability of the Indian summer monsoon. *J. Meteor. Soc. Japan*, **85**, 349–358, doi:10.2151/jmsj.85.349.

——, and ——, 2012: Influence of sea surface temperature on the intraseasonal variability of the South China Sea summer monsoon. *Climate Dyn.*, **39**, 1209–1218, doi:10.1007/s00382-011-1118-x.

——, ——, B. Preethi, P. Terray, and R. Krishnan, 2013: Intraseasonal SST–precipitation relationship and its spatial variability over the tropical summer monsoon region. *Climate Dyn.*, **41**, 45–61, doi:10.1007/s00382-012-1547-1.

Saha, S., and Coauthors, 2010: The NCEP Climate Forecast System Reanalysis. *Bull. Amer. Meteor. Soc.*, **91**, 1015–1057, doi:10.1175/2010BAMS3001.1.

——, and Coauthors, 2014: The NCEP Climate Forecast System version 2. *J. Climate*, **27**, 2185–2208, doi:10.1175/JCLI-D-12-00823.1.

Seo, K. H., J. K. Schemm, W. Wang, and A. Kumar, 2007: The boreal summer intraseasonal oscillation simulated in the NCEP Climate Forecast System: The effect of sea surface temperature. *Mon. Wea. Rev.*, **135**, 1807–1827, doi:10.1175/MWR3369.1.

——, W. Wang, J. Gottschalck, Q. Zhang, J. E. Schemm, W. R. Higgins, and A. Kumar, 2009: Evaluation of MJO forecast skill from several statistical and dynamical forecast models. *J. Climate*, **22**, 2372–2388, doi:10.1175/2008JCLI2421.1.

Sun, J., and H. Chen, 2012: A statistical downscaling scheme to improve global precipitation forecasting. *Meteor. Atmos. Phys.*, **117**, 87–102, doi:10.1007/s00703-012-0195-7.

Waliser, D. E., K.-M. Lau, and J.-H. Kim, 1999: The influence of coupled sea surface temperatures on the Madden–Julian oscillation: A model perturbation experiment. *J. Atmos. Sci.*, **56**, 333–358, doi:10.1175/1520-0469(1999)056<0333:TIOCSS>2.0.CO;2.

——, ——, W. Stern, and C. Jones, 2003: Potential predictability of the Madden–Julian oscillation. *Bull. Amer. Meteor. Soc.*, **84**, 33–50, doi:10.1175/BAMS-84-1-33.

Wang, B., Q. Ding, X. Fu, I. S. Kang, K. Jin, J. Shukla, and F. Doblas-Reyes, 2005: Fundamental challenge in simulation and prediction of summer monsoon rainfall. *Geophys. Res. Lett.*, **32**, L15711, doi:10.1029/2005GL022734.

——, and Coauthors, 2008: How accurately do coupled climate models predict the Asian–Australian monsoon interannual variability? *Climate Dyn.*, **30**, 605–619, doi:10.1007/s00382-007-0310-5.

——, and Coauthors, 2009: Advance and prospectus of seasonal prediction: Assessment of the APCC/CliPAS 14-model ensemble retrospective seasonal prediction (1980–2004). *Climate Dyn.*, **33**, 93–117, doi:10.1007/s00382-008-0460-0.

Wang, W., M. P. Hung, S. J. Weaver, A. Kumar, and X. Fu, 2014: MJO prediction in the NCEP Climate Forecast System version 2. *Climate Dyn.*, **42**, 2509–2520, doi:10.1007/s00382-013-1806-9.

Weisheimer, A., and Coauthors, 2009: ENSEMBLES: A new multi-model ensemble for seasonal-to-annual predictions—Skill and progress beyond DEMETER in forecasting tropical Pacific SSTs. *Geophys. Res. Lett.*, **36**, L21711, doi:10.1029/2009GL040896.

Wen, M., S. Yang, A. Vintzileos, W. Higgins, and R. Zhang, 2012: Impacts of model resolutions and initial conditions on predictions of the Asian summer monsoon by the NCEP Climate Forecast System. *Wea. Forecasting*, **27**, 629–646, doi:10.1175/WAF-D-11-00128.1.

Woolnough, S. J., J. M. Slingo, and B. J. Hoskins, 2000: The relationship between convection and sea surface temperature on intraseasonal timescales. *J. Climate*, **13**, 2086–2104, doi:10.1175/1520-0442(2000)013<2086:TRBCAS>2.0.CO;2.

Wu, R., 2010: Subseasonal variability during the South China Sea summer monsoon onset. *Climate Dyn.*, **34**, 629–642, doi:10.1007/s00382-009-0679-4.

——, B. P. Kirtman, and K. Pegion, 2008: Local rainfall–SST relationship on subseasonal time scales in satellite observations and CFS. *Geophys. Res. Lett.*, **35**, L22706, doi:10.1029/2008GL035883.

Xavier, P. K., J. P. Duvel, and J. D. Francisco, 2008: Boreal summer intraseasonal variability in coupled seasonal hindcasts. *J. Climate*, **21**, 4477–4497, doi:10.1175/2008JCLI2216.1.

Yang, S., Z. Zhang, V. Kousky, R. W. Higgins, S. H. Yoo, J. Liang, and Y. Fan, 2008: Simulations and seasonal prediction of the Asian summer monsoon in the NCEP Climate Forecast System. *J. Climate*, **21**, 3755–3775, doi:10.1175/2008JCLI1961.1.

Zhang, T., S. Yang, X. Jiang, and P. Zhao, 2015: Seasonal–interannual variation and prediction of wet and dry season rainfall over the Maritime Continent: Roles of ENSO and monsoon circulation. *J. Climate*, doi:10.1175/JCLI-D-15-0222.1, in press.

Zhao, S., and S. Yang, 2014: Dynamical prediction of the early season rainfall over southern China by the NCEP Climate Forecast System. *Wea. Forecasting*, **29**, 1391–1401, doi:10.1175/WAF-D-14-00012.1.